Article

Cell Reports

Specific Inhibition of β-Secretase Processing of the Alzheimer Disease Amyloid Precursor Protein

Graphical Abstract

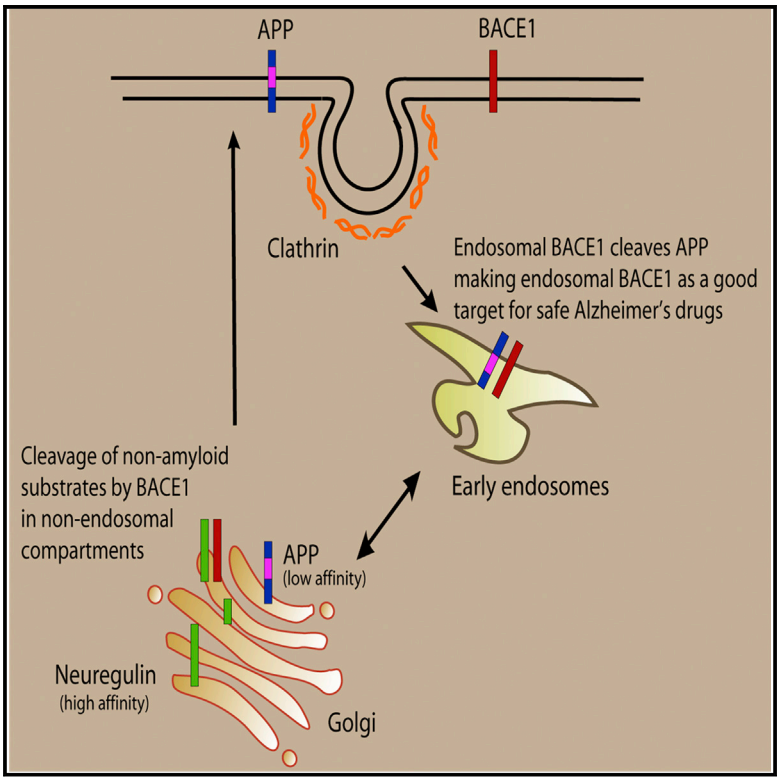

Highlights

- The AD-linked protease BACE1 cleaves APP to produce toxic β-amyloid peptides
- BACE1 also cleaves the non-amyloid substrates NRG1 and L1
- BACE1 cleavage of NRG1 and L1 is endocytosis-independent, unlike the cleavage of APP
- The endosomally targeted BACE1 inhibitor spares NRG1 and L1 but inhibits APP processing

Authors

Saoussen Ben Halima, Sabyashachi Mishra, K. Muruga Poopathi Raja, ..., Christian Haass, Amedeo Caflisch, Lawrence Rajendran

Correspondence

rajendran@bli.uzh.ch

In Brief

Ben Halima et al. demonstrate the feasibility of designing drugs targeting the Alzheimer-related enzyme BACE1 without affecting its physiological function. Using structural, biochemical, and cellular approaches, they show that BACE1 inhibitors can be designed to specifically inhibit its disease-causing activity, enhancing their potential as therapeutics without undesired side effects.

Ben Halima et al., 2016, Cell Reports *14*, 2127–2141
March 8, 2016
http://dx.doi.org/10.1016/j.celrep.2016.01.076

Cell Reports
Article

Specific Inhibition of β-Secretase Processing of the Alzheimer Disease Amyloid Precursor Protein

Saoussen Ben Halima,[1,2,3] Sabyashachi Mishra,[4,12] K. Muruga Poopathi Raja,[5] Michael Willem,[6] Antonio Baici,[4] Kai Simons,[7] Oliver Brüstle,[8,9,10] Philipp Koch,[8] Christian Haass,[6,9,11] Amedeo Caflisch,[4] and Lawrence Rajendran[1,2,3,*]
[1]Systems and Cell Biology of Neurodegeneration, Institute of Regenerative Medicine, University of Zurich, Wagistrasse 12, 8952 Schlieren, Switzerland
[2]Graduate Program in Neuroscience, Neuroscience Center Zurich, 8057 Zurich, Switzerland
[3]Graduate Program of the Zurich Center for Integrative Human Physiology, University of Zurich, 8057 Zurich, Switzerland
[4]Department of Biochemistry, University of Zurich, 8057 Zurich, Switzerland
[5]Department of Physical Chemistry, School of Chemistry, Madurai Kamaraj University, Tamil Nadu 625002, Madurai, India
[6]Biomedical Center, Ludwig-Maximilians-University, 81337 Munich, Germany
[7]Max Planck Institute of Molecular Cell Biology and Genetics, 01307 Dresden, Germany
[8]Institute of Reconstructive Neurobiology, University of Bonn, 53127 Bonn, Germany
[9]German Center for Neurodegenerative Diseases, 53175 Bonn, Germany
[10]Life & Brain, 53127 Bonn, Germany
[11]Munich Cluster for Systems Neurology (SyNergy), 81377 Munich, Germany
[12]Present address: Department of Chemistry, Indian Institute of Technology of Kharagpur, West Bengal 721302, Kharagpur, India
*Correspondence: rajendran@bli.uzh.ch
http://dx.doi.org/10.1016/j.celrep.2016.01.076

SUMMARY

Development of disease-modifying therapeutics is urgently needed for treating Alzheimer disease (AD). AD is characterized by toxic β-amyloid (Aβ) peptides produced by β- and γ-secretase-mediated cleavage of the amyloid precursor protein (APP). β-secretase inhibitors reduce Aβ levels, but mechanism-based side effects arise because they also inhibit β-cleavage of non-amyloid substrates like Neuregulin. We report that β-secretase has a higher affinity for Neuregulin than it does for APP. Kinetic studies demonstrate that the affinities and catalytic efficiencies of β-secretase are higher toward non-amyloid substrates than toward APP. We show that non-amyloid substrates are processed by β-secretase in an endocytosis-independent manner. Exploiting this compartmentalization of substrates, we specifically target the endosomal β-secretase by an endosomally targeted β-secretase inhibitor, which blocked cleavage of APP but not non-amyloid substrates in many cell systems, including induced pluripotent stem cell (iPSC)-derived neurons. β-secretase inhibitors can be designed to specifically inhibit the Alzheimer process, enhancing their potential as AD therapeutics without undesired side effects.

INTRODUCTION

Alzheimer disease (AD) is associated with extracellular deposits of β-amyloid (Aβ) peptide (De Strooper, 2010; Hardy and Higgins, 1992; Tanzi, 2005), which is generated by proteolytic processing of the amyloid precursor protein (APP) by the β-secretase BACE1 (Hussain et al., 1999; Sinha et al., 1999; Vassar et al., 1999; Yan et al., 1999) and γ-secretase. Mutations within the β-cleavage sites of APP can increase the risk for familial forms of AD (Citron et al., 1992; Thinakaran et al., 1996; Zhou et al., 2011) or confer protection against cognitive decline in the elderly (Jonsson et al., 2012), causatively linking BACE1 to AD. Moreover, because of the failure in recent clinical trials of γ-secretase inhibition, mainly because of mechanism-based side effects in humans, BACE1 is considered the preferred drug target (Vassar and Kandalepas, 2011). BACE1 is an attractive therapeutic target for AD. However, complete abolishment of BACE1 activity is associated with specific behavioral and physiological alterations in mice (Cai et al., 2012; Cheret et al., 2013; Hitt et al., 2012; Kim et al., 2007; Lahiri et al., 2014; Li and Südhof, 2004). These alterations may arise from the failure to process some non-amyloid BACE1 substrates such as NRG1, which is involved in axonal myelination of neurons (Hu et al., 2006, 2010; Ma et al., 2007; Willem et al., 2006); immunoglobulin (Ig)-containing β1 Nrg1 (IgNrg1β1) (Cheret et al., 2013); the β2 subunit voltage-gated sodium channel (Nav1β2) (Kim et al., 2007; Wong et al., 2005); and axon guidance molecules, including CHL1 (Rajapaksha et al., 2011) and L1 (Zhou et al., 2012), Jagged (Hu et al., 2013), β-galactoside α 2, 6-sialyltransferase (ST6Gall) (Kitazume et al., 2005; Sugimoto et al., 2007), APLP1 and APLP2 (Li and Südhof, 2004), lipoprotein receptor-related protein (LRP) (von Arnim et al., 2005), interleukin 1 receptor II (IL-1R2, but not tumor necrosis factor α [TNF-α]) (Kuhn et al., 2007, 2012), and vascular endothelial growth factor receptor 1 (VEGFR1) (Cai et al., 2012). Therefore, a general BACE1 inhibitor might block cleavage of non-amyloid substrates, decreasing its value as an AD therapeutic drug (Cai et al., 2012; Cheret et al., 2013; Hitt et al., 2012; Kim et al., 2007; Lahiri et al., 2014; Li and Südhof, 2004).

In the cell, proteins are distributed to multiple subcellular locations (Mellman and Nelson, 2008). Spatial distribution of proteins is crucial for spatial cellular functions (Rajendran and Simons, 2005). In polarized cells such as neurons, cellular distribution of proteins allows temporal and spatial control of diverse cellular functions. Many cellular proteins show multiple subcellular locations, such as BACE1. BACE1 is located in the *trans*-Golgi network (TGN) (Yan et al., 2001), plasma membrane (Walter et al., 2001a, 2001b), and early endosomes (Rajendran et al., 2006) and in polarized cells such as neurons because these cells also display compartmentalization of BACE1 in axons versus somatodendritic compartments (Buggia-Prévot et al., 2014; Vassar et al., 2014). BACE1 cleaves APP in early endosomes after endocytosis (Rajendran et al., 2006). Both the enzyme and the substrate undergo endocytosis, presumably through different routes, and meet in early endosomes for processing (Rajendran et al., 2006; Sannerud et al., 2011; Schneider et al., 2008). Currently it is unknown whether non-amyloid substrates such as NRG1 or L1 are processed in the endosomal compartment or other compartments. Selectively inhibiting the activity of BACE1 in a particular subcellular compartment, early endosomes, where it cleaves APP, could be an effective therapeutic strategy provided the other substrates are cleaved in non-endosomal compartments. Therefore, in this work, we explored the compartmentalization of BACE1 substrate processing to address the feasibility of targeting BACE1 for inhibition in the subcellular compartment, where it cleaves the APP substrate.

We studied the expression profiles of BACE1 substrates. Indeed, RT-PCR analysis of many BACE1 substrates, including APP and NRG1, revealed their expression throughout the mouse lifespan (Figure S1A), suggesting that general BACE1 inhibition could affect the processing of both amyloid and non-amyloid substrates at all stages. Whether an inhibitor could be developed to specifically target APP cleavage and, thereby, minimize non-specific side effects is currently unclear. We explored the possibility of specifically inhibiting β-cleavage of APP, but not that of non-amyloid substrates, by assessing its distinct structural, biochemical and, cellular requirements.

RESULTS

Molecular Dynamics Simulations Suggest that NRG1 Is a Better Substrate Than WT APP for BACE1

To characterize BACE1 interaction with non-amyloid versus amyloid substrates, we designed eight-residue P4-P4′ peptides as substrates based on the BACE1 binding regions from wild-type (WT) APP, NRG1, and P-selectin glycoprotein ligand 1 (PSGL1, [SELPLG1]) for structural and biochemical analyses (Figure S1B; Hu et al., 2006; Lichtenthaler et al., 2003; Willem et al., 2006). The corresponding peptide sequence derived from the Swedish mutant of the amyloid precursor protein (swAPP), a familial mutation that causes early-onset AD (Citron et al., 1992) and differs by only two residues from WT APP and binds BACE1 better, was used as a positive control (Hong et al., 2000). The corresponding substrate analog inhibitors were derived by replacing the scissile peptide bond with an isostere moiety, which renders the peptide bond non-cleavable.

To this end, we first performed explicit solvent molecular dynamics (MD) simulations of the BACE1/substrate complexes (Figures 1A and 1B; Figure S1C) and BACE1/substrate analog inhibitors (Figure S2A) based on the BACE1-OM99 inhibitor complex (Hong et al., 2000). The ensemble-averaged interaction energies and their electrostatic and van der Waals contributions were determined. We found that the overall plasticity of the BACE1 protein was essentially the same in all MD runs irrespective of the substrate to which it was bound (Figure S2). As anticipated, the interaction energy for BACE1 with swAPP was more favorable than with WT APP (Barman et al., 2011; Hong et al., 2000; Figure 1B).

Unexpectedly, MD simulations indicated that BACE1 interacts more favorably with the non-amyloid substrate NRG1 than with either amyloid substrate (Figure 1B). Furthermore, a higher affinity of BACE1 for NRG1 than WT APP and swAPP was also observed in MD simulations carried out with the substrate analog inhibitors (Figure S2). The range of values of the electrostatic contribution for the four different substrates was about an order of magnitude larger than the van der Waals range (400 kcal/mol versus 40 kcal/mol, respectively) and therefore dominated the variation in the total interaction energy (which is the sum of these two terms). The individual contributions of each of the P4-P4′ residues of the substrates showed that the Glu residues at (P2) and (P2′) of NRG1 are involved in more favorable interactions with BACE1 than the corresponding residues in WT APP and PSGL1 (Figures 1A and 1C; Figure S1C). We observed that this could be due to salt bridge interactions of the P2 and P2′ Glu residues in NRG1 with Arg235 and Arg128 of BACE1, respectively (Figure 1A). This observation suggested that the replacement of the acidic Glu to a basic amino acid in the substrate would be unfavorable because this will inhibit the formation of the electrostatic interaction between the substrate and the enzyme. Indeed, in WT APP, a Lys residue is present at the (P2) position, which creates an unfavorable interaction with BACE1, presumably because of the proximity of the side chain of Arg235 (Figure 1A).

To ascertain the individual contributions of the P2 and P2′ Glu side chains of NRG1, simulations were carried out with mutants containing Lys instead of Glu at both sites or only at (P2). The interaction energy of the single (P2) mutant was weakened almost as much as for the double mutant, which suggests that the Glu at (P2) site alone contributes significantly to the interaction with BACE1 and much more than the Glu at (P2′) (Figure 1C). Further, we replaced the Lys at (P2) in WT APP with Glu and found that this substitution conferred a higher affinity for BACE1 (Figure 1B). Therefore, position (P2) strongly affects the substrate affinity for BACE1 through the formation of favorable (NRG1) or unfavorable (WT APP) interactions (Figure 1C). These results also revealed additional information: it is the presence of the (P2) Lys that renders WT APP a weaker substrate rather than the acquisition of the dipeptide segment Asn-Leu at (P2)-(P1), which makes the Swedish mutant of APP a better substrate (Figure 1C; Figure S2; Barman et al., 2011; Hong et al., 2000). Interestingly, another non-amyloid substrate, L1, also harbors a similar acidic amino acid (Glu) and may potentially interact with the Arg235 in BACE1 (Zhou et al., 2012).

Therefore, MD simulations of BACE1 binding to amyloid as well as the non-amyloid substrate NRG1 uncovered the

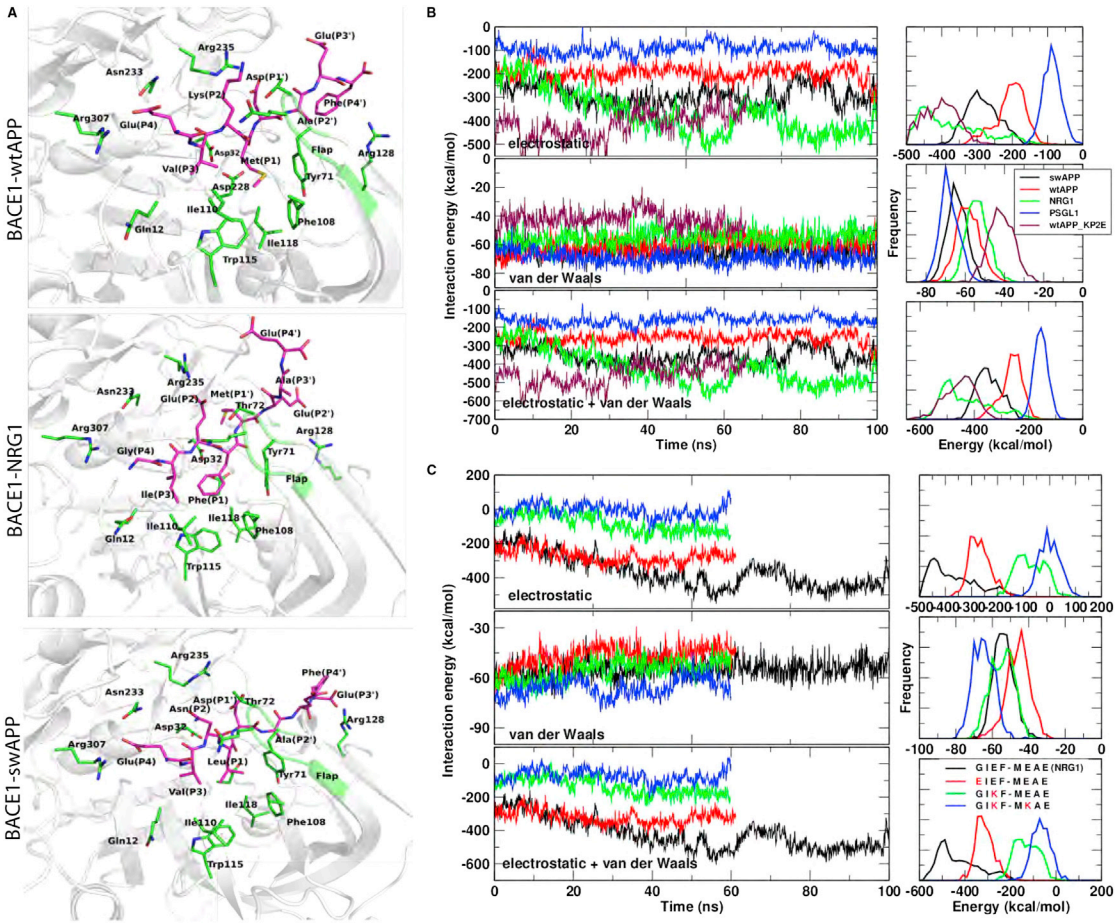

Figure 1. Molecular Dynamics Simulation Predicts that NRG1 Is a Better Substrate Than WT APP for BACE1

(A) The active site of BACE1 with the octapepetide substrates of WT APP, NRG1, and swAPP. The snapshot for each BACE1-substrate complex shown is the representative structure of the most populated conformer, which was obtained by clustering all MD snapshots by root-mean-square deviation and a cutoff of 0.8 Å. All C_α atoms of BACE1, except for the loops A, C, D, and F, were used in the structural fitting prior to the clustering. The flap is shown as a ribbon and the side chains of BACE1 and substrate as sticks. The carbon atoms of substrate are shown in magenta for clarity.

(B) Time series of interaction energy between BACE1 and the four substrates (swAPP, WT APP, NRG1, and PSGL1 are shown in black, red, green, and blue, respectively) and the K(P2)E mutant of WT APP (maroon). The order of the stabilizing interaction was as follows: NRG1 > WT APP K(P2)E mutant > swAPP > WT APP > PSGL1.

(C) Time series of the interaction of BACE1 with NRG1 and its three mutants. The stabilizing interaction by P2 (Glu) is more significant than that of P2′ (Glu). The order of the stabilizing interaction was as follows: NRG1 (black) > NRG1 G(P4)E (red) > NRG1 E(P2)K (green) > NRG1 E(P2K) E(P2′)K (blue).

See also Figures S1, S2, and S3.

importance of the critical acidic residue (P2) Glu of NRG1 in conferring a stable interaction with BACE1.

In Vitro Fluorescence Experiments Demonstrate that NRG1 Is a Better Substrate Than APP

To experimentally test the predictions of MD simulations and to evaluate the potency of amyloid and non-amyloid substrate analog inhibitors, we used the cell-free fluorescence resonance energy transfer (FRET)-based BACE1 activity assay (Ermolieff et al., 2000). We quantified the effect of the different substrate analog inhibitors on BACE1 cleavage of a fluorophore quencher-labeled, WT-APP-based peptide FRET reporter (Figure 2A; Figure S3). As a positive control for inhibition, we used the BACE1 inhibitor C3. We found that the NRG1-derived inhibitor reduced BACE1 cleavage with comparable efficiency to that of an swAPP-derived inhibitor (Figure 2A), confirming the simulation predictions. In contrast, the WT APP-derived inhibitor was less effective at reducing BACE1 activity, and the PSGL1-based inhibitor resembled that of control condition with no inhibition of the fluorescence readouts (Figure 2A). Similar results were obtained with a fluorophore quencher-labeled, NRG1-based peptide FRET reporter (Figure 2B). Therefore, at least in vitro, BACE1 binds NRG1 with a higher affinity than WT APP.

The (P2) Glu Residue in the Binding Site of NRG1 Confers High-Affinity Binding to BACE1

To understand whether BACE1 not only binds but also cleaves NRG1 better than WT APP, we determined the hydrolytic

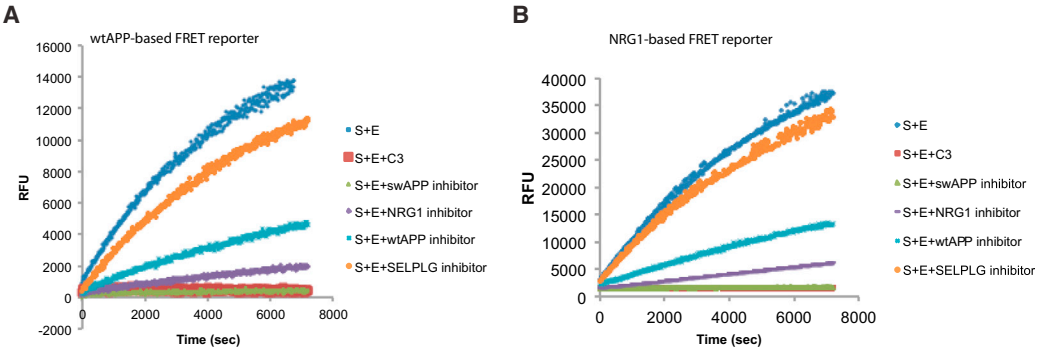

C

	V ($\mu M\ S^{-1}$)	K_m (μM)	K_{cat} (S^{-1})	K_{cat}/K_m ($M^{-1}\ S^{-1}$)
APP	$(5.0 \pm 0.1) \times 10^{-4}$	36 ± 3.6	$(2.08 \pm 0.04) \times 10^{-3}$	57.8 ± 5.9
swAPP	$(6.0 \pm 0.5) \times 10^{-3}$	5.2 ± 1.2	$(2.5 \pm 0.2) \times 10^{-2}$	4800 ± 1200
NRG1	$(2.7 \pm 0.1) \times 10^{-3}$	19.6 ± 2.8	$(1.12 \pm 0.04) \times 10^{-2}$	570 ± 80

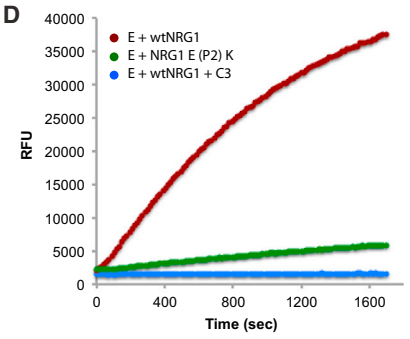

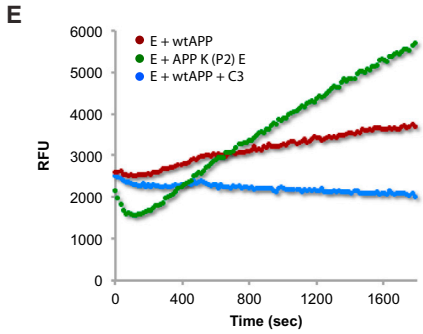

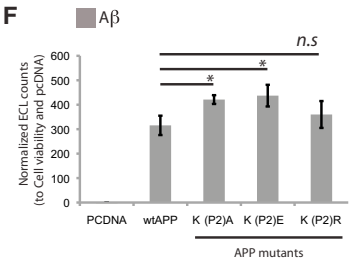

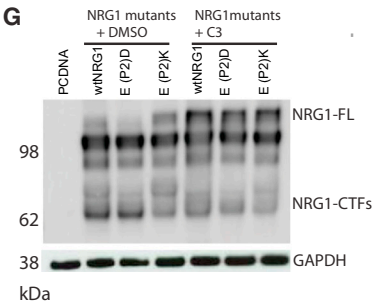

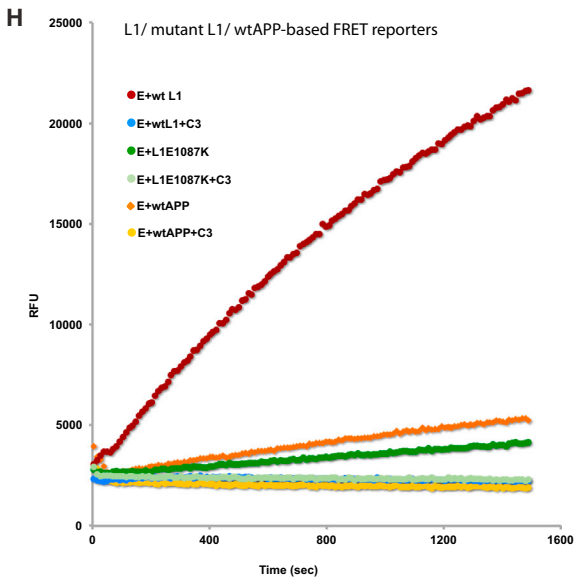

(legend on next page)

efficiency of BACE1 for the amyloid and non-amyloid substrates and used swAPP as a positive control. We calculated K_M and k_{cat} values to determine the affinity and cleavage efficiencies, respectively, with specificity defined by k_{cat}/K_M values. The affinity of BACE1 for NRG1 was twice that for WT APP (K_M of 19.6 ± 2.8 μM and 36.6 ± 3.6 μM, respectively). As predicted, swAPP displayed a low K_M value of 5.2 μ± 1.2 μM. BACE1 cleaved WT APP with the lowest specificity, represented by a k_{cat}/K_M value of 57.8 ± 5.9 M^{-1} S^{-1}, whereas it cleaved NRG1 with a specificity of 570 ± 80 M^{-1} S^{-1}, which is 10-fold higher than WT APP. In contrast, swAPP was cleaved with the highest specificity of 4,800 ± 1,200 M^{-1} S^{-1} (Figure 2C; Figure S4). Finally, compared with WT APP, the catalytic efficiency of BACE1 was approximately five times higher for NRG1 and ten times higher for swAPP. Therefore, NRG1 is a better substrate for BACE1 than WT APP.

Because MD simulations suggested that NRG1 binds BACE1 with higher affinity, and because this is most likely due to the (P2) Glu residue in NRG1, we wanted to verify this experimentally. We replaced the (P2) Glu residue of NRG1 with a Lys residue (NRG1 E(P2)K) to mimic WT APP (P2) and found that this substitution reduced the rate of cleavage by BACE1 (Figure 2D). On the other hand, exchanging the Lys residue of WT APP (P2) for a Glu residue (WT APP K(P2)E) increased the rate of cleavage (Figure 2E). Therefore, the (P2) Glu residue of NRG1 makes it a significantly better substrate for BACE1 than WT APP both in terms of binding and cleavage efficiency.

To evaluate the importance of the residue at (P2) for cleavage by BACE1 in the cellular context, we replaced the Lys with Glu at this position in WT APP and transfected this construct into HEK cells stably expressing BACE1. Consistent with the in vitro results, this substitution conferred increased Aβ production (Figure 2F). Interestingly, replacement of the (P2) Lys with a smaller, non-charged Ala residue also increased Aβ production (Figure 2F) suggesting that a Lys residue at (P2) interferes with the binding to BACE1, as suggested by the MD simulations. Substitution of (P2) Lys with another basic amino acid, Arg, did not alter Aβ levels (Figure 2F). On the other hand, substitution of the (P2) Glu in NRG1 with the basic residue Lys but not with another acidic residue, Asp, dramatically decreased its cleavage by BACE1 in cells (Figure 2G). C3 inhibited processing of all mutants (Figure 2G), demonstrating that their cleavages are BACE-dependent. Therefore, these data unequivocally demonstrate that the Glu residue in the cleavage site of NRG1 plays a critical role in the affinity and cleavage efficiency of BACE1 both in vitro and in cells.

BACE1 Displays Higher Cleavage Efficiencies toward Another Non-amyloid Substrate, L1

The non-amyloid substrate of BACE1, L1, also has a Glu residue in the BACE1 cleavage site (Zhou et al., 2012) and, therefore could confer a higher affinity to BACE1 binding and cleavage efficiency. To test this, we evaluated the BACE1 cleavage kinetics of L1 with and without the critical Glu residue mutated (Figure 2H). Indeed, similar to NRG1, wild-type L1 was processed with higher cleavage efficiency than WT APP (Figure 2H). Interestingly, mutating the Glu residue to Lys nearly abolished the cleavage by BACE1 (Figure 2H). As expected, the cell-permeable inhibitor C3 abolished BACE1 cleavage of all substrates. Therefore, BACE1 has a higher affinity and catalytic efficiency toward the non-amyloid substrates such as NRG1 and L1 than toward WT APP.

β-Cleavage of the Non-amyloid Substrates NRG1 and L1 Does Not Require Endocytosis

Despite being a poor substrate (Grüninger-Leitch et al., 2002; Sauder et al., 2000), and even in the presence of the higher-affinity substrates, APP is cleaved in the cellular context and also in vivo. We hypothesized that BACE1 cleaves different substrates in distinct subcellular compartments. For instance, previous work has shown that swAPP, which has a higher affinity for BACE1, is cleaved by β-secretase in the biosynthetic compartments (Haass et al., 1995; Thinakaran et al., 1996), whereas

Figure 2. BACE1 Displays Higher Cleavage Efficiencies toward the Non-amyloid Substrates NRG1 and L1

(A and B) Kinetics of the binding of WT APP (A) and NRG1 (B) to BACE1. The inhibitory potential of each of the substrate analog inhibitors (NRG1 [purple], WT APP [light blue], PSGL1/SELPLG1 [yellow], and swAPP [green])-statine is assayed in a BACE1 cell-free assay using either WT APP (A) or NRG1 (B) as a reporter for BACE1 activity (dark blue). C3 is used as the BACE inhibitor (orange). Note that the swAPP-derived inhibitor (green curve) is as efficient as C3. RFU, relative fluorescence unit; S, substrate; E, enzyme; SELPLG, selectin-P ligand.

(C) Values of the kinetics parameters (V, K_M, k_{cat}, k_{cat}/K_M) of BACE1 binding to WT APP and swAPP and NRG1 BACE1 cleavage site-derived substrate peptides. NRG1 is cleaved with higher affinity and higher cleavage efficiency than WT APP by BACE1. See also Figure S4.

(D) Cleavage efficiencies of BACE1 toward NRG1 and mutant NRG1 E(P2)K. An in vitro BACE1 activity assay was performed using wild-type NRG1 (red) FRET substrate versus mutant NRG1 (E(P2)K) FRET substrate (green). The kinetic reactions are inhibited by the addition of C3 as a control, confirming the specificity of the BACE1-dependent activity assay (blue).

(E) Cleavage efficiencies of BACE1 toward WT APP and mutant APP K(P2)E. An in vitro BACE1 activity assay was performed using wild-type APP (red) FRET substrate versus mutant APP FRET substrate (green). The kinetic reactions are inhibited by the addition of C3 as a control, confirming the specificity of the BACE1-dependent activity assay (blue).

(F and G) The position (P2) in the substrate cleavage site plays a role in BACE1 cleavages of APP and NRG1.

(F) HEK293 stably expressing BACE1 cells transfected with either PCDNA, WT APP, mutant K(P2)A, mutant K(P2)E, or mutant K(P2)R. Cell culture supernatants were assayed for Aβ40 and measured by electrochemiluminescence (ECL) assay (Bali et al., 2012). The K(P2)A and K(P2)E mutants produced significantly more Aβ40 than the wild-type. p values are 0.013 (K(P2)A), 0.023 (K(P2)E), and 0.3184 (K(P2)R). Error bars indicate SD. ns, not significant.

(G) HEK293 stably expressing BACE1 cells transfected with either PCDNA, NRG1 wild-type, mutant E(P2)D NRG1, and mutant E(P2)K NRG1 and then treated with DMSO or the BACE1 inhibitor C3. Cell lysates were separated on SDS-PAGE gel and evaluated by western blot with Sc-348 antibody. Note that, with the BACE1 inhibitor C3, the accumulation of the mature band of NRG1 is observed in all mutants.

(H) L1 is a better substrate than WT APP. An in vitro BACE1 activity assay was performed using wild-type L1 (red) FRET substrate versus mutant L1 FRET substrate (dark green). The kinetic reactions are inhibited by the addition of C3 as a control, confirming the specificity of the BACE1-dependent activity assay (WT L1 + C3 [blue], mutant L1 + C3 [light green], and WT APP with [light yellow filled circle] and without C3 [orange filled triangle]).

cleavage of WT APP occurs in endosomes (Carey et al., 2005; Koo and Squazzo, 1994; Rajendran and Annaert, 2012; Rajendran et al., 2006; Udayar et al., 2013). Because our findings show that NRG1 also has a higher affinity for BACE1 than WT APP, we hypothesized that NRG1 might also be processed independent of endocytosis. To determine whether β-cleavage of NRG1 is similar or different to that of WT APP in terms of its requirement of endocytosis, we perturbed membrane trafficking pathways and assessed the β-cleavage of NRG1. Expression of dominant-negative dynamin (Dyn K44A), a mutant of the GTPase involved in fission of the endocytic vesicles that inhibits dynamin-dependent endocytosis, did not inhibit the cleavage of NRG1 (Figure 3A). Similarly, pharmacological inhibition of clathrin-dependent/clathrin-independent endocytosis using Pitstop2 (Dutta et al., 2012; Stahlschmidt et al., 2014; von Kleist et al., 2011), an inhibitor that inhibits clathrin-mediated endocytosis and clathrin-independent endocytosis, did not inhibit the cleavage of NRG1 (Figure 3A). However, both treatments significantly inhibited β-cleavage of APP and Aβ production (Figure 3B). Pitstop2 had a more pronounced effect on Aβ than secreted APPβ (sAPPβ), probably because of the inhibition of γ-secretase internalization as well as inhibition of BACE1 endocytosis. Control experiments showed that, indeed, treatment of cells with Pitstop2 (Figure 3C) or cells expressing Dynamin K44A inhibited endocytosis of Transferrin (Figures 3C and 3D) and epidermal growth factor (EGF) (Figure 3C), two clathrin/dynamin-dependent cargoes. Therefore, unlike APP, NRG1 does not require endocytosis for cleavage by BACE1.

Consistent with these observations and similar to NRG1, L1 was also cleaved by BACE1 in an endocytosis-independent manner (Figure 3E) suggesting that unlike APP, the other physiologically relevant substrates may not require dynamin/clathrin endocytosis for their β-cleavages and providing further support to the idea that BACE1 cleaves these higher affinity substrates in an endocytosis-independent manner.

The Endosomally Targeted, Sterol-Linked BACE1 Inhibitor Inhibits Aβ Production and Cleavage of APP without Affecting β-Cleavage of NRG1 and L1

Exploiting the observation that different membrane trafficking pathways differentially regulate β-cleavage of APP and NRG1 or L1, we tested whether inhibiting BACE1 activity specifically in the endosomal compartment would inhibit β-cleavage of APP and, thereby, spare the cleavage of the non-amyloid substrates NRG1 and L1. We found that the cell-permeable pan inhibitor C3 substantially inhibited β-cleavage of NRG1 in cells, whereas an endosomally targeted, sterol-linked BACE1 inhibitor (Rajendran et al., 2008) showed no significant inhibition of NRG1 β-cleavage (Figures 4A and 4B). However, both treatments inhibited β-cleavage of WT APP and Aβ production (Figure 4C). Similar results were obtained in primary mouse neuronal cultures, where an endosomally targeted, sterol-linked inhibitor of β-secretase spared cleavage of NRG1 but not of APP (Figure S5) under an endogenous BACE1 expression level.

Similar to NRG1, we then tested whether BACE1-mediated cleavage of L1, which also did not require endocytosis, could be spared by using the endosomally targeted, sterol-linked BACE1 inhibitor. Treatment with the endosomally targeted, sterol-linked BACE1 inhibitor did not affect β-cleavage of L1, whereas treatment with the general cell-permeable BACE1 inhibitor C3 abolished almost all BACE1 processing (Figures 4D and 4E). In control experiments performed with APP, β-cleavage of WT APP was inhibited completely by both the endosomally targeted, sterol-linked BACE1 inhibitor and the general cell-permeable inhibitor (Figure 4C).

The Endosomally Targeted, Sterol-Linked BACE1 Inhibitor Inhibits NRG1 Processing When Subcellular Compartmentalization Is Compromised

To test whether the endosomally targeted, sterol-linked BACE1 inhibitor can indeed inhibit NRG1 processing when the integrity of subcellular compartmentalization is compromised, we tested the effect of both BACE1 inhibitors: the endosomally targeted, sterol-linked inhibitor and the cell-permeable pan inhibitor C3 on solubilized membranes and assessed inhibition of NRG1 cleavage. Under these conditions, where cellular compartmentalization is compromised, both the endosomally targeted, sterol-linked BACE1 inhibitor and C3 significantly blocked BACE1 cleavage of NRG1 (Figure 5A). These results suggest that subcellular compartmentalization of different substrates in endosomal and non-endosomal compartments contributes to the differential processing of these substrates by BACE1.

Among the non-endosomal compartments that harbor β-secretase activity, the TGN and the plasma membrane have been suggested to be places for β-secretase activity (Li and Südhof, 2004; Prabhu et al., 2012). To investigate whether the processing of NRG1 by BACE1 occurs at the cell surface, we used a cell-impermeable BACE1 inhibitor, GL189 (Capell et al., 2002), and tested its inhibitory potential on BACE1 cleavage of NRG1. This inhibitor is a substrate analog transition state inhibitor that has been demonstrated to bind to active BACE1 in solubilized membrane fraction assays (Capell et al., 2002). Therefore, we hypothesized that, if active BACE1 is present at the cell surface that is competent to cleave NRG1, then this cell-impermeable transition state inhibitor should inhibit BACE1 cleavage of NRG1. However, treatment of cells expressing NRG1 with GL189 did not inhibit the processing of NRG1 by BACE1 (Figure 5B). However, the control C3, the cell-permeable BACE1 inhibitor, almost abolished the processing of NRG1 by BACE1 (Figure 5B). Similarly, endocytosis inhibition also did not inhibit BACE1 processing of NRG1. However, addition of C3 under endocytosis inhibition inhibits NRG1 cleavage, demonstrating that NRG1 cleavage occurs neither at the plasma membrane nor in endosomes (Figure 5B). As additional controls, we also checked whether BACE1 cleavage of APP was affected under similar conditions and found that treatment of cells with the cell-impermeable inhibitor GL-189 had no effect on β-cleavage of APP. However, treatment with the endocytosis inhibitor or cell-permeable inhibitor or both inhibited β-cleavage, showing conclusively that β-cleavage of APP does not occur at the plasma membrane but is dependent on endocytosis. Taken together, these results indicate that BACE1 cleaves NRG1 neither at the plasma membrane nor in endosomes but, most likely, at the TGN, the only other low-pH, non-endo-lysosomal organelle that is conducive for BACE1 activity.

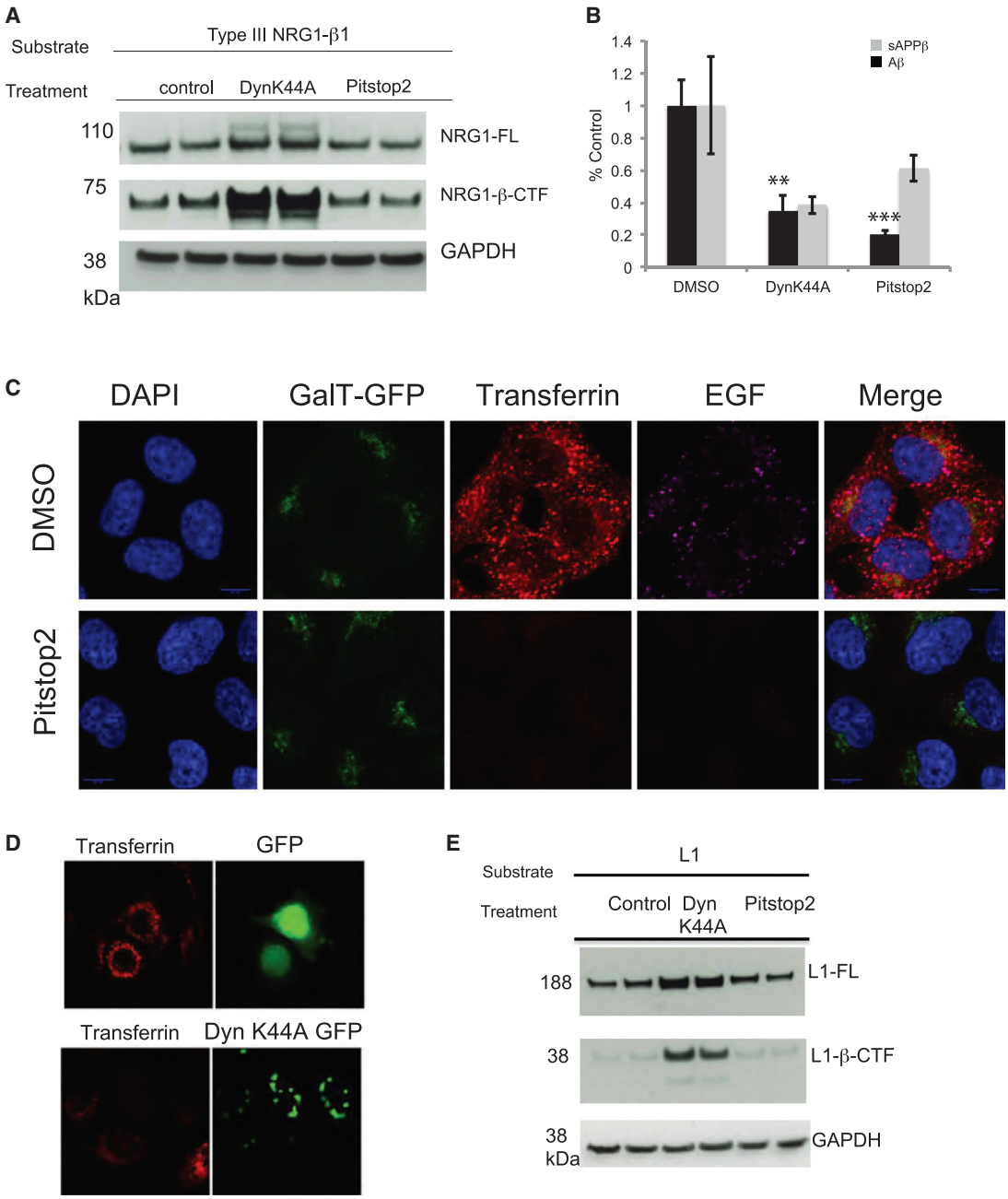

Figure 3. β-Cleavage of the Non-amyloid Substrates NRG1 and L1 Does Not Require Endocytosis

(A) β-Cleavage of NRG1 is independent of dynamin/clathrin-mediated endocytosis. HEK293 stably expressing BACE1 cells were co-transfected with either NRG1β1 type III and GFP or NRG1β1 type III and dynamin dominant-negative mutant (Dyn K44A) or transfected with NRG1β1 type III and GFP and treated with Pitstop2. Western blot analysis of lysates to detect full-length (FL) NRG1 with Sc-348 antibody and NRG1-β-CTF using the neo-epitope antibody 4F10. Note the stabilization of NRG1 full-length and NRG1-β-CTF upon Dyn K44A co-transfection.

(B) HEK293 stably expressing BACE1 cells were co-transfected with DynK44A and WT APP or transfected with WT APP and treated with Pitstop2, Aβ40, and sAPPβ were measured from cell media using an ECL assay (Bali et al., 2012), with p values of 0.006 for DynK44A (Aβ40) and 0.002 for Pitstop2 (Aβ40).

(C) Treatment of cells with clathrin/dynamin inhibitors inhibits endocytosis of Transferrin and EGF. HeLa-GalT-GFP cells were treated with the solvent control (DMSO) or with Pitstop2 and incubated with Transferrin (red) and EGF (magenta). Scale bars, 10 μm. Confocal Leica SP8, 63× 3.15 zoom.

(D) Dynamin K44A inhibits Transferrin endocytosis. HeLa cells were transfected with either control GFP (green, top) or Dynamin K44A GFP (bottom) and incubated with Transferrin (red).

(E) L1 β-cleavage is independent of dynamin/Clathrin-mediated endocytosis. HEK293 stably expressing BACE1 were co-transfected with either L1 and GFP or L1 and Dyn K44A or transfected with L1 and GFP and treated with Pitstop2. Western blot analysis of the lysate detects full-length L1 and L1-β-CTF with PcytL1 antibody. Again, note the stabilization of L1 full-length and L1-β-CTF upon Dyn K44A co-transfection, similar to NRG1.

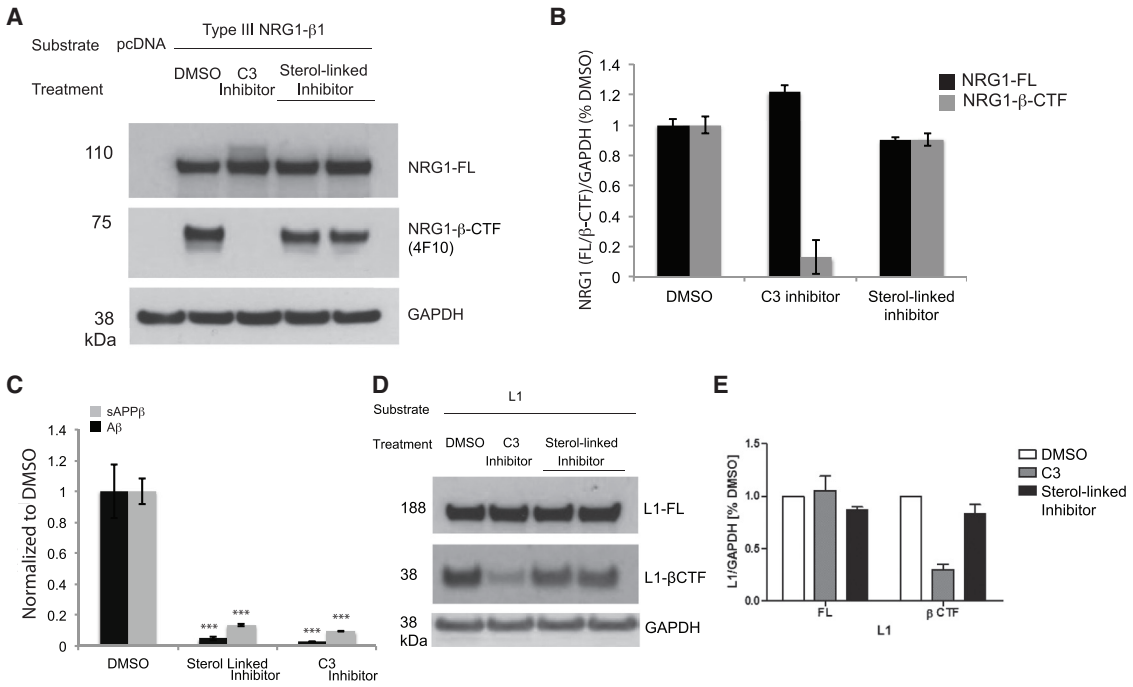

Figure 4. The Endosomally Targeted, Sterol-Linked BACE1 Inhibitor Inhibits Aβ Production and Cleavage of APP without Affecting Cleavage of NRG1 and L1

(A) The endosomally targeted, sterol-linked inhibitor spares NRG1 processing in cells. HEK293 stably expressing BACE1 cells were transfected with NRG1 β1 type III and treated with DMSO as a control, with the cell-permeable BACE1 inhibitor C3, or with the endosomally targeted, sterol-linked BACE1 inhibitor. Western blot analysis of lysates detects full-length NRG1 with Sc-348 antibody and NRG1-β-CTF using the neo-epitope antibody 4F10. A representative western blot is shown.

(B) Semiquantification of western blots. Data were mean ± S.E. (n = 3). Student's t test was used to calculate p values: C3-FL, 0.427; C3-β-CTF (β-cleaved C-terminal fragment), 0.0075; endosomally targeted, sterol-linked BACE1 inhibitor-FL, 0.882; endosomally targeted, sterol-linked BACE1 inhibitor-β-CTF, 0.488.

(C) The endosomally targeted, sterol-linked BACE1 inhibitor inhibited APP processing. HEK293 stably expressing BACE1 were transfected with WT APP and treated with DMSO as a control, with the cell-permeable BACE1 inhibitor C3, or with the endosomally targeted, sterol-linked BACE1 inhibitor for 12 hr. Aβ40 and sAPPβ were measured from cell media using an ECL assay. The values represent experimental triplicates. p values for the sterol-linked inhibitor for sAPPβ and Aβ40 are 0.0009 and 0.0021, respectively. *P*-values for the C3 inhibitor for sAPPβ and Aβ40 are 0.0006 and 0.0020, respectively. Error bars indicate SD.

(D) The endosomally targeted, sterol-linked inhibitor spares L1 processing in cells. HEK293 stably expressing BACE1 cells were transfected with L1 and treated with DMSO as a control, with the cell-permeable BACE1 inhibitor C3, or with the endosomally targeted, sterol-linked BACE1 inhibitor. Western blot analysis of lysates with PcytL1 antibody detects full-length L1 and L1-β-CTF.

(E) Semiquantification of western blots. Data were mean ± SE (n = 3). Student's t test was used to calculate the p values: C3-FL, 0.0169; C3-β-CTF, 0.0022; endosomally targeted, sterol-linked BACE1 inhibitor-FL, 0.4975; endosomally targeted, sterol-linked BACE1 inhibitor-β-CTF, 0.187.

The Endosomally Targeted, Sterol-Linked BACE1 Inhibitor Inhibits APP Processing without Affecting NRG1 Processing in iPSC-Derived Human Neurons

To validate the findings regarding the endosomally targeted, sterol-linked BACE1 inhibitor sparing NRG1 cleavage in a more relevant setting for potential treatment in AD patients, we treated neurons generated from human induced pluripotent stem cells (h-iPSCs) derived from healthy human donors (Figure 6A; Figure S6) with C3, the cell-permeable BACE1 inhibitor, or the endosomally targeted, sterol-linked BACE1 inhibitor and assayed for BACE1 processing of NRG1 and APP (as a control) in those cells. C3 BACE1 inhibitor treatment inhibited BACE1 processing of NRG1 (Figures 6B and 6C). Treatment with the endosomally targeted, sterol linked BACE1 inhibitor did not affect the processing of NRG1 by BACE1 (Figures 6B and 6C). However, upon C3 BACE1 inhibitor and endosomally targeted, sterol-linked inhibitor treatment, both Aβ40 and sAPPβ were reduced dramatically, with sAPPα levels increased (Figure 6D).

The Endosomally Targeted, Sterol-Linked BACE1 Inhibitor Is Targeted to Endocytic Compartments but Not to the Golgi

Consistent with these results, the fluorescently labeled, sterol-linked inhibitor trafficked to endosomal compartments (Figures 7A and 7B) but not to the *trans*-Golgi network, where high-affinity substrates could be cleaved (Haass et al., 1995; Thinakaran et al., 1996), as judged by the colocalization experiments (Figure 7C). When incubated on cells, the fluorescently labeled, sterol-linked inhibitor trafficked from the plasma membrane to EEA1-positive early endosomes (Figure 7A), the compartments shown previously to be important for β-cleavage of APP, and then was transported retrogradely to late endosomal/lysosomal compartments at longer periods of incubation, as demonstrated by colocalization with Lamp1 (Figure 7B). The endosomally targeted, sterol-linked inhibitor did not traffic to the TGN 30 min to 1 hr after uptake, as shown by the absence of localization between the inhibitor and GalT-GFP, a Golgi-resident protein

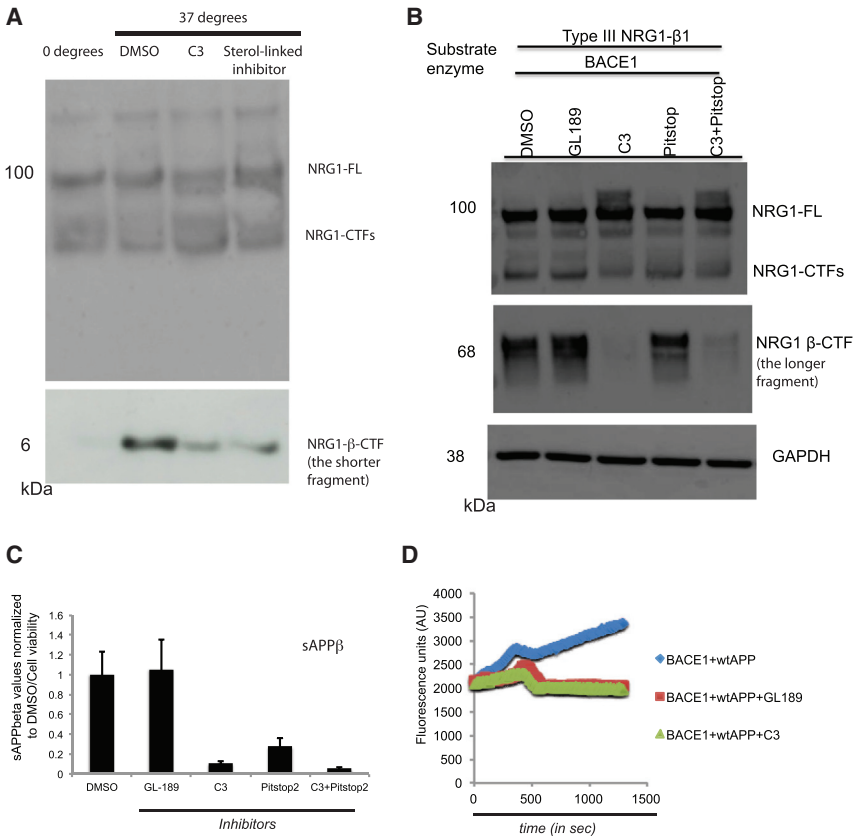

Figure 5. The Endosomally Targeted, Sterol-Linked BACE1 Inhibitor Inhibits β-Cleavage of NRG1 When Subcellular Compartmentalization Is Compromised and β-Cleavage of NRG1 Does Not Occur at the Cell Surface

(A) BACE1 activity and inhibition by C3, a cell permeable BACE inhibitor, and the endosomally targeted, sterol-linked BACE1 inhibitor in solubilized membranes. Shown is a western blot analysis of solubilized membrane from HEK293 cells stably expressing BACE1 and transfected with NRG1 β1 type III. The membrane BACE1 activity assay was carried out at 37°C and 0°C for the control. The cell-permeable C3 inhibitor and the endosomally targeted, sterol-linked BACE1 inhibitor were used to inhibit BACE1 activity toward NRG1 at 37°C. DMSO is used as a solvent control. Full-length and NRG1-CTFs are detected with Sc-348 antibody. NRG1-β-CTF is detected by 4F10 antibody (neo-epitope-specific antibody).

(B) Western blot analysis of cell expressing NRG1 β1 type III and treated with DMSO as a control, the cell-permeable BACE1 inhibitor C3, the cell-impermeable transition state BACE1 inhibitor GL189, and the endocytosis inhibitor Pitstop2 or co-treated with Pitstop2 and C3. Full-length (NRG1-FL) and NRG1-CTFs are detected with Sc-348 antibody. NRG1-β-CTF is detected by 4F10 antibody (neo-epitope-specific antibody).

(C) β-Cleavage of APP does not occur at the cell surface. Supernatants of cells expressing APP were subjected to an ECL assay to measure sAPPβ to determine the effect of cell-permeable (C3), cell-impermeable (GL-189), and endocytosis inhibitor (Pitstop2) on the β-cleavage of APP. Values were normalized to cell viability and to DMSO-treated cells.

(D) In vitro BACE1 FRET assay to assess the inhibitory potential of the cell non-permeable BACE1 inhibitor GL189 (red), the cell-permeable BACE1 inhibitor C3 (green), and DMSO (blue) as the control reaction. The y axis displays the relative fluorescence units, and the x axis displays time in seconds. The reaction is depicted from time = 200 s.

(Figure 7C). As a control, Shiga toxin, a TGN-dedicated cargo, promptly colocalized with GalT-GFP (Figure 7D). This shows that the endosomally targeted, sterol-linked inhibitor confines itself to the endocytic pathway that is involved in Aβ production. Therefore, an endosomally targeted, sterol-linked BACE1 inhibitor specifically inhibited APP cleavage, which predominantly occurs in endosomal compartments, and spared the processing of other substrates (L1 and NRG1) that are cleaved independent of endocytosis. These results provide strong evidence that inhibition of BACE1 cleavage of APP is feasible without interfering with the cleavage of non-amyloid substrates, as shown here for NRG1 and L1.

Our results suggest that subcellular compartmentalization allows BACE1 to cleave APP in the endosomal compartment and other non-amyloid substrates in non-endosomal compartments. However, substrates could also be compartmentalized in different domains at the membrane level. Cell membranes are not homogenous in their lipid and protein distribution, and certain lipids, such as cholesterol and sphingolipid, tend to form dynamic nanoassemblies (Simons and Ikonen, 1997). Because the endosomally targeted, sterol-linked BACE1 inhibitor not only is endocytosis-competent but can also compartmentalize into lipid raft domains, we asked whether the specific inhibition is due to the fact that only APP cleavage was endocytosis-dependent or because only APP is partitioned into lipid rafts. Although our endocytosis inhibition experiment clearly pointed out that the subcellular compartmentalization of substrates is the reason, we tested this possibility if only APP was partitioned into lipid rafts and if this is the reason for specific inhibition with the endosomally targeted, sterol-linked BACE1 inhibitor. To this end, we studied the distribution of APP, BACE1, NRG1, and L1 in detergent-resistant microdomains (DRMs), a biochemical way of isolating such membrane domains. We isolated DRMs we identified using standard protocols (Rajendran et al., 2003; Figure S7). Western blot analysis of the lipid rafts revealed that APP and BACE1 strongly localize in those domains as reported by several groups (Figure S7). In compliance with our endocytosis inhibition data, we found that both NRG1 and L1 full-length and C-terminal fragment (CTF) were also localized in DRMs, similar to APP and BACE1. These results indicate that lipid raft localization is not the mechanism behind the sparing of BACE1 processing of NRG1 and L1 by the endosomally targeted, sterol-linked BACE1 inhibitor but, rather, compartmentalization into endosomal versus non-endosomal compartments.

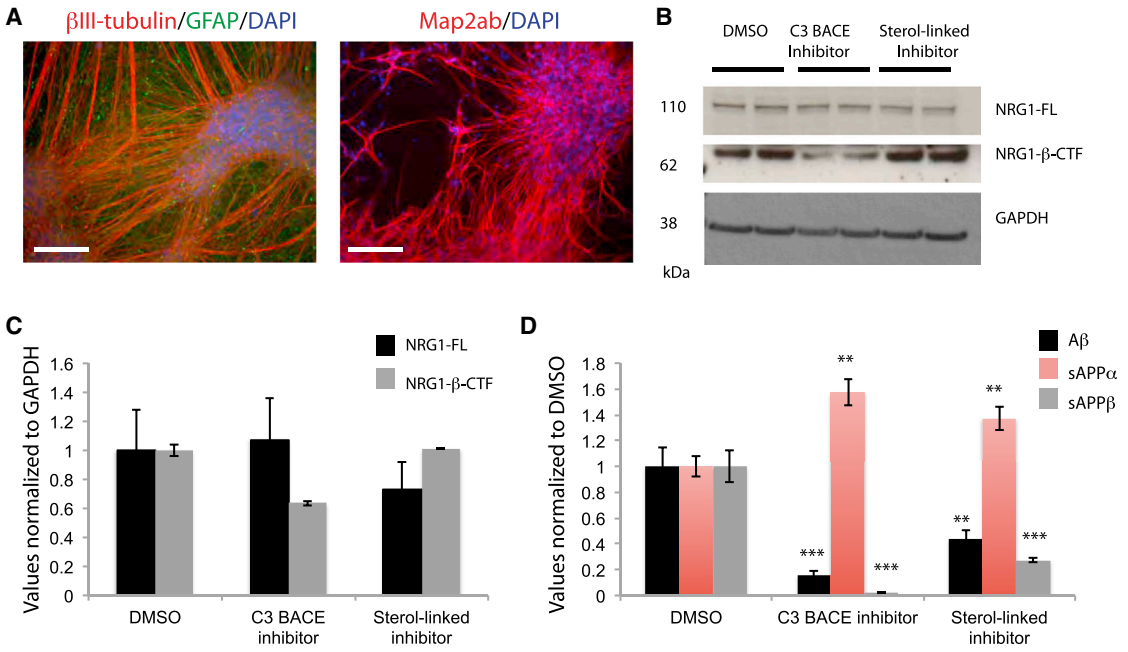

Figure 6. The Endosomally Targeted, Sterol-Linked BACE1 Inhibitor Reduces β-Cleavage of APP and Aβ Production in Human iPSC-Derived Neurons but Not that of NRG1.

(A) Induced pluripotent stem cell-derived differentiated cultures consist of a dominant fraction of neurons expressing β-III tubulin (red, left) and Map2ab (red, right). A smaller percentage of GFAP-expressing astrocytes is also present in the cultures (green, left). Scale bars, 200 μm.

(B) NRG1 processing in human iPSC-derived neurons is inhibited upon treatment with C3 and endosomally targeted, sterol-linked BACE1 inhibitor. Human iPSC-derived neurons were treated with 5 μM of the BACE1 inhibitor C3, 100 nM of endosomally targeted, sterol-linked BACE1 inhibitor, or DMSO as a control for 22 hr. Cell lysates were subjected to western blot analysis using SC348 antibody to detect full-length NRG1 and 4F10 antibody to detect NRG1-β-CTF.

(C) Semiquantification of the blot.

(D) Cell supernatants were subjected to an ECL assay to measure Aβ40, sAPPβ, and sAPPα. Values were normalized to protein concentration and to DMSO-treated cells. The values represent experimental triplicates. p values for the endosomally targeted, sterol-linked inhibitor for Aβ40, sAPPβ, and sAPPα are 0.00138, 0.00888, and 3.82×10^{-6}, respectively. p values for the C3 inhibitor for Aβ40, sAPPβ, and sAPPα are 9.41×10^{-5}, 0.00248, and 8.06×10^{-6}, respectively. Error bars indicate SD.

See also Figures S5 and S6.

DISCUSSION

Inhibition of BACE1 is being pursued intensively as a therapeutic target to treat AD, and BACE1 inhibitors are currently in clinical trials (Vassar et al., 2014). However, mechanism-based toxicity might arise from inhibition of BACE1. Chemical inhibition of BACE1 in adult animals has been shown to alter maintenance of muscle spindles (Cheret et al., 2013) and to impair synaptic functions (Filser et al., 2015). Therefore, it is essential to consider other strategies to design more selective BACE1 inhibitors that specifically inhibit APP cleavage and Aβ production. In this work, we explored the differential subcompartmentalization of substrate processing as a strategy to increase the selectivity of BACE1 inhibitors. We show that the cleavage of high-affinity, non-amyloid substrates by BACE1 does not require dynamin/clathrin-mediated endocytosis, whereas processing of APP does. Our results point to the importance of the acidic residue in the BACE1 binding site of the substrate at the P2 position. Even before BACE1 was identified, Citron et al. (1995) predicted the importance of the P2 residue in APP, and we now show that, for non-amyloid substrates, the presence of an acidic residue confers high-affinity binding. This may be a mechanism used by BACE1 to be able to process its high- and low-affinity substrates in different compartments; namely, non-amyloid substrates in the non-endosomal compartments such as the TGN and APP in endosomes. An alternative explanation could be the protonation of the Glu residues in NRG1/L1 in low pH of the endosomes that inhibits its cleavage in endosomes, which could also explain why swAPP cleavage by BACE1, which does not have the Glu residue in this position, is still partly dependent on endocytosis.

One other possibility is that APP is cleaved in the endosomal compartment that is regulated by clathrin and/or dynamin, whereas other substrates are cleaved in a still unidentified endosomal compartment that is independent of clathrin/dynamin. However, our observations point out the existence of distinct subcellular compartments where APP and other physiological substrates are cleaved by BACE1. Exploiting this differential subcellular compartmentalization of BACE1 processing, we specifically targeted WT APP processing with an endosomally targeted, sterol-linked BACE1 inhibitor. Although the design of the inhibitor to target endosomal BACE1 has been described previously (Rajendran et al., 2008), our data show the utility of this inhibitor as a tool to distinguish BACE1 cleavage of APP

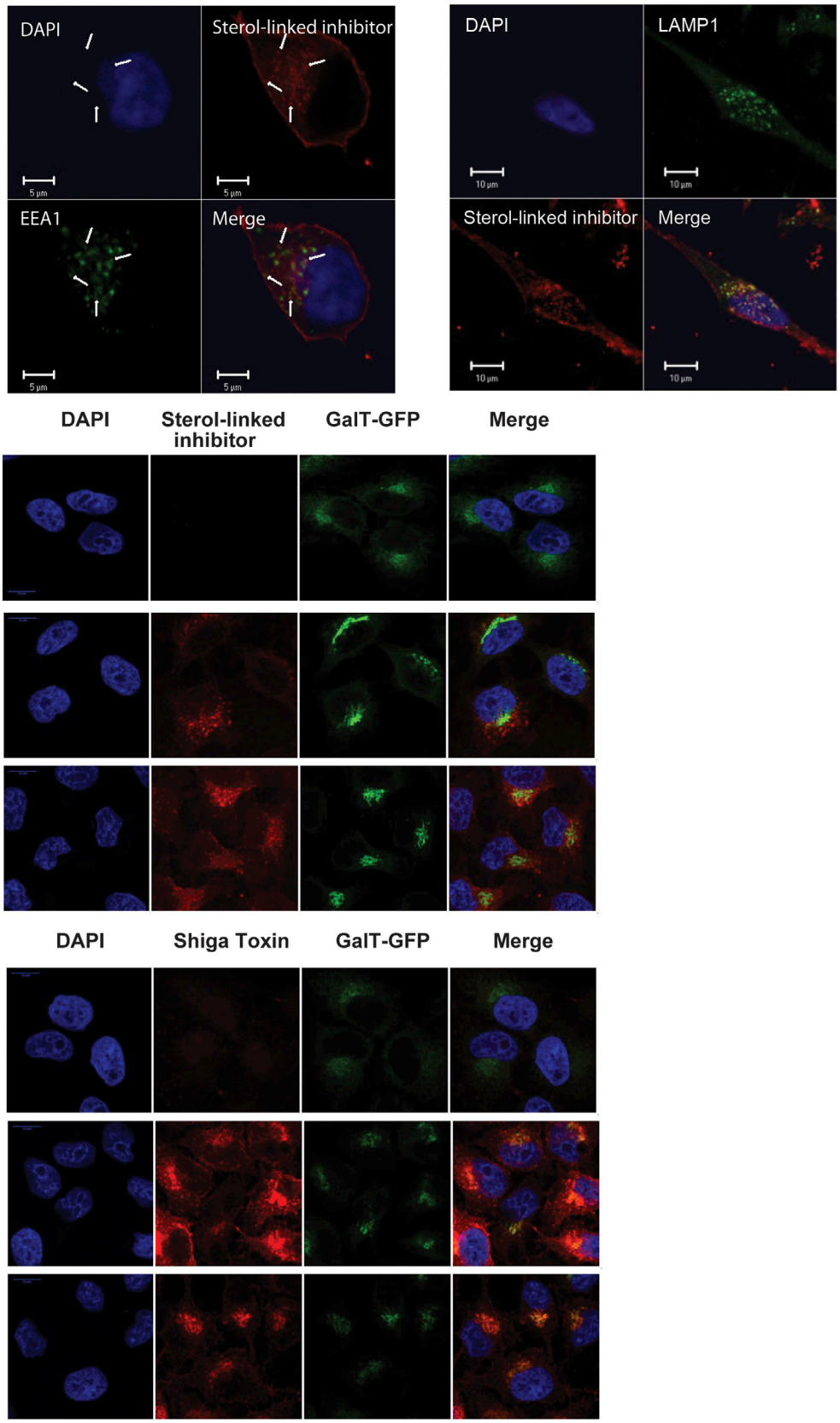

(legend on next page)

and non-amyloid substrates because of the subcellular compartmentalization of these cleavages. An alternative possibility for the mode of action of the endosomally targeted, sterol-linked BACE1 inhibitor is that the endosomally targeted inhibitor, because of its sterol linkage, targets APP cleavage that occurs in lipid rafts of endosomes (Ehehalt et al., 2003) and, therefore, spares non-amyloid substrates that could be localized in non-raft domains in the endosomes. However, for this to occur, NRG1 processing must be endocytosis-dependent, and its processing should occur in non-raft domains of endosomes. By using Pitstop2, an inhibitor of clathrin-dependent and -independent endocytosis (Dutta et al., 2012; Stahlschmidt et al., 2014; von Kleist et al., 2011), and also with dominant-negative dynamin, we clearly demonstrate that, although APP processing by BACE1 requires endocytosis, β-cleavage of the non-amyloid substrates NRG1 and L1 does not require endocytosis. This suggests that the NRG1/L1-sparing activity of the endosomally targeted, sterol-linked BACE1 inhibitor is most likely due to endosomal targeting and not due to differential localization of these non-amyloid substrates in non-raft domains of the endosomes. Moreover, in our experiments with isolated DRMs, all substrates are localized in DRMs as well. Therefore, our results point out that only APP β-cleavage occurs in endosomes and, therefore, encourages the possibility that endosomally targeted BACE1 therapeutic substances can reduce Aβ production without affecting other BACE1 substrate cleavages. Endosomally targeted BACE1 inhibitors are potential therapeutic substances for the specific treatment of AD without adverse effects.

The limitations of our study include the lack of translation in animal models because these are beyond the scope of this study, but our experiments on human iPSCs provides hope. Clearly, further research is needed to translate these findings in experimental animals and also patients. Regardless, our work demonstrates that inhibiting Aβ production without affecting BACE1 processing of other substrates is possible and of important clinical value for the specific treatment of AD.

EXPERIMENTAL PROCEDURES

MD Simulations

For the MD simulations, the initial structure of the BACE1-substrate complex was obtained from the crystal structure of the ecotodomain of BACE1 bound to the OM99-2 inhibitor (Glu-Val-Asn-Leu-φ[CHOH-CH2]-Ala-Ala-Glu-Phe), where φ[CHOH-CH2] represents a hydroxyethylene isostere of the peptide bond (PDB: 1FKN) (Hong et al., 2000). The hydroxyethylene isostere was replaced by a carbonyl group to obtain the peptide bond and all MD simulations were carried out with peptide substrates. The OM99-2 inhibitor corresponds to the swAPP sequence with the Asp(P1′)Ala mutation. The original form of the swAPP sequence was obtained by mutating Ala at P1′ of OM99-2 to Asp. From the structure of the swAPP substrate, the initial structures of WT APP (Glu-Val-Lys-Met-Asp-Ala-Glu-Phe), NRG1 (Gly-Ile-Glu-Phe-Met-Glu-Ala-Glu), and PSGL1 (Ala-Ser-Asn-Leu-Ser-Val-Asn-Tyr) substrates were obtained by appropriate mutations. The BACE-substrate complexes were immersed in a cubic water box of size 93 A. The initial structures were equilibrated for 2-ns and 100-ns MD trajectories were calculated for each of the four BACE-substrate complexes at constant temperature (300 K) and pressure (1 atm) employing the NAMD program (Phillips et al., 2005) with the CHARMM22 force field (MacKerell et al., 1998) and TIP3 potential for water molecules (Jorgensen et al., 1983). The procedure was repeated for the three mutants of NRG1, i.e., NRG1 G(P4)E, NRG1 E(P2)K, NRG1 E(P2′)K, and the K(P2)E mutant of WT APP. For each these four mutants, 60 ns MD trajectories were calculated. Similarly, we performed 60 ns of MD simulations for the four BACE-inhibitor complexes where the hydroxyethylene isostere of the peptide bond was retained (data not shown). Here we considered the Ala(P1′) residue of OM99-2 for a direct comparison with in vitro assays. In addition, a 120-ns MD run was performed for each of the complexes between BACE1 and the statine-based (hydroxyethylene isostere) inhibitors. The P4-P4′ residues were extracted from the sequences of swAPP (OM99-2 inhibitor), WT APP, NRG1, and PSGL1, except for the Ala at P1′, which was kept as in OM99-2 for all four inhibitors.

Cell-free BACE1 Activity Assay

The cell-free BACE1 activity assay was performed in a final volume of 100 μl in assay buffer: 50 mM sodium acetate (pH 4.5) and 0.1% Triton X-100. 0.24 μM of recombinant human BACE1-ectodomain (rhBACE1) (Sigma S4195) was mixed with 10 μM of each substrate in a flat-bottom black 96-wells plate (Nunc 237105). The assay was performed at 37 ± 1°C with excitation and emission wavelengths set at 340 nm and 400 nm, respectively. For cell-free BACE1 activity assay with inhibtors, 0.24 μM of rhBACE1 was incubated with 10 μM of each inhibitor for 10 min at 37°C in the assay buffer prior to the addition of each substrate.

K_m and K_{cat} Measurements and Calculations

The specificity of the different substrates for rhBACE1 was kinetically assayed by measuring the Michaelis constant K_m and the limiting rate V, from which the specificity constant K_{cat}/K_m was calculated. Instability of the enzyme during assay was assessed with the Selwyn test (Selwyn, 1965). Fluorescence measurements were performed in a final volume of 100 μl using flat bottomed black 96-well plates in a Tecan Infinite M1000Pro microplate reader thermostatted at 37 ± 1°C with excitation and emission wavelengths of 340 nm and 400 nm, respectively. Readings were performed in kinetic mode for 5 min, during which time fluorescence increased linearly. For a constant 0.24 μM enzyme concentration, 5 or 6 substrate concentrations covering approximately the range 0.2 to 5 K_m, as determined in preliminary experiments, were used. Stock solutions of the substrates were prepared in pure DMSO, but the concentration of the organic solvent was kept constant at 1% v/v for all substrate concentrations. Only for the swAPP substrate, the final DMSO concentration was 2% v/v. The buffer was 50 mM sodium acetate (pH 4.5) with 0.1% Triton X-100 added. K_m and V were calculated by non-linear regression fitting of the Michaelis-Menten equation.

Quantitative Measurements of Aβ40, sAPPβ and sAPPα

Human Aβ40, human sAPPβ, human sAPPα, and mouse Aβ40 were assayed from supernatants, after centrifugation at 1,000 rpm for 3 min, using the electrochemiluminescence (ECL) assay as described in Bali et al., 2012.

Primary Neuronal Culture, Transduction and Inhibitors Treatments

Mixed cortical/hippocampal neurons were prepared from embryonic day 15 and 16 mice. In brief, dissociated cells were plated onto 6-well poly-D-lysine-coated

Figure 7. Trafficking of the Endosomally Targeted, Sterol-Linked BACE1 Inhibitor

(A and B) Uptake of the rhodamine-conjugated, endosomally targeted, sterol-linked inhibitor (red) and colocalization with EEA1 (green) after 5 min of internalization (A) and with Lamp-1 (green) after 15 min of internalization (B) in HeLa cells.

(C) HeLa-GalT-GFP cells were incubated with rhodamine-conjugated, endosomally targeted, sterol-linked BACE1 inhibitor (red) and GalT-GFP (green) for different times (0, 30, and 60 min). Scale bar, 10 μm. Confocal Leica SP8, 63× 3.15 zoom.

(D) Similarly, HeLa-GalT-GFP cells were incubated with Shiga toxin (red) and GalT-GFP (green) for different times (0, 30, and 60 min). Scale bar, 10 μm. Confocal Leica SP8, 63× 3.15 zoom.

dishes at a density of ~250.000/cm^2 and cultured in Neurobasal medium (Invitrogen) with B27 supplements (Invitrogen), 2mM L-glutamine, and penicillin/streptomycin. After 5 days, in vitro neuronal cultures were incubated with lentiviral NRG1 β1 type III or GFP particles for 8 hr. 48 hr after transduction, cells were treated with DMSO or inhibitors (C3, TAPI-1 and the endosomally-targeted sterol-linked BACE1 inhibitor) for 24 hr, as previously described.

iPSC-Derived Neuronal Cultures and Treatment

Human iPSC-derived long-term self-renewing neuroepithelial stem cells (lt-NES cells) (Mertens et al., 2013) were maintained in DMEM/F12, 2 mM L-glutamine, 1.6 g/l glucose, 0.1 mg/ml penicillin/streptomycin, N2 supplement (Life Technologies), B27 (1 μl/ml; Life Technologies), and fibroblast growth factor 2 (FGF2) and epidermal growth factor (EGF; both 10 ng/ml; Cell Guidance Systems) on tissue culture plates coated with poly-L-ornithine/laminin (both Sigma), and passaged every 3 or 4 days. Neuronal differentiation was induced by withdrawal of FGF2 and EGF in differentiation media (MACS Neuro Medium supplemented with MACS NeuroBrew-21 (1:50; Miltenyi Biotec) and DMEM/ F12 supplemented with N2 mixed at a 1:1 ratio) that was exchanged every other day. C3 BACE1 inhibitor (5 μM), endosomally-targeted sterol-linked BACE1 inhibitor (100 nM), or DMSO solvent control were added to neuronal cultures differentiated for 4 weeks. Cultures were incubated for 22 hr before supernatant and protein lysates were collected.

Statistical Analysis

All data are shown as mean ± SD. Two-tailed Student's t test was used for comparison of the means between two groups. *$p < 0.05$, **$p < 0.005$, and ***$p < 0.0005$.

SUPPLEMENTAL INFORMATION

Supplemental Information includes Supplemental Experimental Procedures and seven figures and can be found with this article online at http://dx.doi.org/10.1016/j.celrep.2016.01.076.

AUTHOR CONTRIBUTIONS

L.R. designed the research. S.B.H. and M.W. performed the biochemistry and cell biological experiments. S.M. and A.C. analyzed the MD simulations. A.B. helped with the kinetics experiments. K.M.P.R. synthesized the statine-based inhibitors. All authors participated in designing the experiments and in data analysis. L.R. and S.B.H. wrote the paper, and all authors participated in the editing of the paper. P.K. and O.B. contributed to the iPSC experiments.

ACKNOWLEDGMENTS

We thank T. Südhof, M. Schwab, A. Aguzzi, G. Jennings, H. Knoelker, and U. Konietzko for their input. We gratefully acknowledge the help of Jado Technologies GmbH with synthesis of the sterol-linked BACE1 inhibitors. We thank E. Schwarz and S. Hoey for critical reading of the manuscript. We thank U. Konietzko for the APP-HA tag plasmids, B. de Strooper for the L1 plasmid, P. Altevogt for the anti-L1 antibody, L. Johannes for the fluorescently labeled Shiga toxin B subunit, G. Siegel for the preparation of primary mice neurons, Z. Goodger and J. Ries for help with RT-PCR analysis, and H. Schwalbe for allowing us to use the instrument facility. L.R. acknowledges financial support from Swiss National Science Foundation grants, the Velux Foundation, the Cure Alzheimer Fund, the Baugarten Stiftung, and the Bangerter Stiftung. P.K. and O.B. acknowledge financial support from the German Federal Ministry for Education and Research (BioPharma-NeuroAllianz Grant 0315608A). A.C. acknowledges financial support from the Swiss National Science Foundation.

Received: April 15, 2013
Revised: November 9, 2015
Accepted: January 26, 2016
Published: February 25, 2016

REFERENCES

Bali, J., Gheinani, A.H., Zurbriggen, S., and Rajendran, L. (2012). Role of genes linked to sporadic Alzheimer's disease risk in the production of β-amyloid peptides. Proc. Natl. Acad. Sci. USA *109*, 15307–15311.

Barman, A., Schürer, S., and Prabhakar, R. (2011). Computational modeling of substrate specificity and catalysis of the β-secretase (BACE1) enzyme. Biochemistry *50*, 4337–4349.

Buggia-Prévot, V., Fernandez, C.G., Riordan, S., Vetrivel, K.S., Roseman, J., Waters, J., Bindokas, V.P., Vassar, R., and Thinakaran, G. (2014). Axonal BACE1 dynamics and targeting in hippocampal neurons: a role for Rab11 GTPase. Mol. Neurodegener. *9*, 1.

Cai, J., Qi, X., Kociok, N., Skosyrski, S., Emilio, A., Ruan, Q., Han, S., Liu, L., Chen, Z., Bowes Rickman, C., et al. (2012). β-Secretase (BACE1) inhibition causes retinal pathology by vascular dysregulation and accumulation of age pigment. EMBO Mol. Med. *4*, 980–991.

Capell, A., Meyn, L., Fluhrer, R., Teplow, D.B., Walter, J., and Haass, C. (2002). Apical sorting of beta-secretase limits amyloid beta-peptide production. J. Biol. Chem. *277*, 5637–5643.

Carey, R.M., Balcz, B.A., Lopez-Coviella, I., and Slack, B.E. (2005). Inhibition of dynamin-dependent endocytosis increases shedding of the amyloid precursor protein ectodomain and reduces generation of amyloid beta protein. BMC Cell Biol. *6*, 30.

Cheret, C., Willem, M., Fricker, F.R., Wende, H., Wulf-Goldenberg, A., Tahirovic, S., Nave, K.A., Saftig, P., Haass, C., Garratt, A.N., et al. (2013). Bace1 and Neuregulin-1 cooperate to control formation and maintenance of muscle spindles. EMBO J. *32*, 2015–2028.

Citron, M., Oltersdorf, T., Haass, C., McConlogue, L., Hung, A.Y., Seubert, P., Vigo-Pelfrey, C., Lieberburg, I., and Selkoe, D.J. (1992). Mutation of the beta-amyloid precursor protein in familial Alzheimer's disease increases beta-protein production. Nature *360*, 672–674.

Citron, M., Teplow, D.B., and Selkoe, D.J. (1995). Generation of amyloid beta protein from its precursor is sequence specific. Neuron *14*, 661–670.

De Strooper, B. (2010). Proteases and proteolysis in Alzheimer disease: a multifactorial view on the disease process. Physiol. Rev. *90*, 465–494.

Dutta, D., Williamson, C.D., Cole, N.B., and Donaldson, J.G. (2012). Pitstop 2 is a potent inhibitor of clathrin-independent endocytosis. PLoS ONE *7*, e45799.

Ehehalt, R., Keller, P., Haass, C., Thiele, C., and Simons, K. (2003). Amyloidogenic processing of the Alzheimer beta-amyloid precursor protein depends on lipid rafts. J. Cell Biol. *160*, 113–123.

Ermolieff, J., Loy, J.A., Koelsch, G., and Tang, J. (2000). Proteolytic activation of recombinant pro-memapsin 2 (Pro-beta-secretase) studied with new fluorogenic substrates. Biochemistry *39*, 16263.

Filser, S., Ovsepian, S.V., Masana, M., Blazquez-Llorca, L., Brandt Elvang, A., Volbracht, C., Müller, M.B., Jung, C.K., and Herms, J. (2015). Pharmacological inhibition of BACE1 impairs synaptic plasticity and cognitive functions. Biol. Psychiatry *77*, 729–739.

Grüninger-Leitch, F., Schlatter, D., Küng, E., Nelböck, P., and Döbeli, H. (2002). Substrate and inhibitor profile of BACE (beta-secretase) and comparison with other mammalian aspartic proteases. J. Biol. Chem. *277*, 4687–4693.

Haass, C., Lemere, C.A., Capell, A., Citron, M., Seubert, P., Schenk, D., Lannfelt, L., and Selkoe, D.J. (1995). The Swedish mutation causes early-onset Alzheimer's disease by beta-secretase cleavage within the secretory pathway. Nat. Med. *1*, 1291–1296.

Hardy, J.A., and Higgins, G.A. (1992). Alzheimer's disease: the amyloid cascade hypothesis. Science *256*, 184–185.

Hitt, B., Riordan, S., Kukreja, L., Eimer, W., Rajapaksha, T., and Vassar, R. (2012). β-Site amyloid precursor protein (APP)-cleaving enzyme 1 (BACE1)-deficient mice exhibit a close homolog of L1 (CHL1) loss-of-function phenotype involving axon guidance defects. J. Biol. Chem. *287*, 38408–38425.

Hong, L., Koelsch, G., Lin, X., Wu, S., Terzyan, S., Ghosh, A.K., Zhang, X.C., and Tang, J. (2000). Structure of the protease domain of memapsin 2 (beta-secretase) complexed with inhibitor. Science *290*, 150–153.

Hu, X., Hicks, C.W., He, W., Wong, P., Macklin, W.B., Trapp, B.D., and Yan, R. (2006). Bace1 modulates myelination in the central and peripheral nervous system. Nat. Neurosci. *9*, 1520–1525.

Hu, X., Zhou, X., He, W., Yang, J., Xiong, W., Wong, P., Wilson, C.G., and Yan, R. (2010). BACE1 deficiency causes altered neuronal activity and neurodegeneration. J. Neurosci. *30*, 8819–8829.

Hu, X., He, W., Luo, X., Tsubota, K.E., and Yan, R. (2013). BACE1 regulates hippocampal astrogenesis via the Jagged1-Notch pathway. Cell Rep. *4*, 40–49.

Hussain, I., Powell, D., Howlett, D.R., Tew, D.G., Meek, T.D., Chapman, C., Gloger, I.S., Murphy, K.E., Southan, C.D., Ryan, D.M., et al. (1999). Identification of a novel aspartic protease (Asp 2) as beta-secretase. Mol. Cell. Neurosci. *14*, 419–427.

Jonsson, T., Atwal, J.K., Steinberg, S., Snaedal, J., Jonsson, P.V., Bjornsson, S., Stefansson, H., Sulem, P., Gudbjartsson, D., Maloney, J., et al. (2012). A mutation in APP protects against Alzheimer's disease and age-related cognitive decline. Nature *488*, 96–99.

Jorgensen, W.L., Chandrasekhar, J., Madura, J.D., Impey, R.W., and Klein, M.L. (1983). Comparison of Simple Potential Functions for Simulating Liquid Water. J. Chem. Phys. *79*, 926–935.

Kim, D.Y., Carey, B.W., Wang, H., Ingano, L.A., Binshtok, A.M., Wertz, M.H., Pettingell, W.H., He, P., Lee, V.M., Woolf, C.J., and Kovacs, D.M. (2007). BACE1 regulates voltage-gated sodium channels and neuronal activity. Nat. Cell Biol. *9*, 755–764.

Kitazume, S., Nakagawa, K., Oka, R., Tachida, Y., Ogawa, K., Luo, Y., Citron, M., Shitara, H., Taya, C., Yonekawa, H., et al. (2005). In vivo cleavage of alpha2,6-sialyltransferase by Alzheimer beta-secretase. J. Biol. Chem. *280*, 8589–8595.

Koo, E.H., and Squazzo, S.L. (1994). Evidence that production and release of amyloid beta-protein involves the endocytic pathway. J. Biol. Chem. *269*, 17386–17389.

Kuhn, P.H., Marjaux, E., Imhof, A., De Strooper, B., Haass, C., and Lichtenthaler, S.F. (2007). Regulated intramembrane proteolysis of the interleukin-1 receptor II by alpha-, beta-, and gamma-secretase. J. Biol. Chem. *282*, 11982–11995.

Kuhn, P.H., Koroniak, K., Hogl, S., Colombo, A., Zeitschel, U., Willem, M., Volbracht, C., Schepers, U., Imhof, A., Hoffmeister, A., et al. (2012). Secretome protein enrichment identifies physiological BACE1 protease substrates in neurons. EMBO J. *31*, 3157–3168.

Lahiri, D.K., Maloney, B., Long, J.M., and Greig, N.H. (2014). Lessons from a BACE1 inhibitor trial: off-site but not off base. Alzheimers Dement. *10* (*5, Suppl*), S411–S419.

Li, Q., and Südhof, T.C. (2004). Cleavage of amyloid-beta precursor protein and amyloid-beta precursor-like protein by BACE 1. J. Biol. Chem. *279*, 10542–10550.

Lichtenthaler, S.F., Dominguez, D.I., Westmeyer, G.G., Reiss, K., Haass, C., Saftig, P., De Strooper, B., and Seed, B. (2003). The cell adhesion protein P-selectin glycoprotein ligand-1 is a substrate for the aspartyl protease BACE1. J. Biol. Chem. *278*, 48713–48719.

Ma, H., Lesné, S., Kotilinek, L., Steidl-Nichols, J.V., Sherman, M., Younkin, L., Younkin, S., Forster, C., Sergeant, N., Delacourte, A., et al. (2007). Involvement of beta-site APP cleaving enzyme 1 (BACE1) in amyloid precursor protein-mediated enhancement of memory and activity-dependent synaptic plasticity. Proc. Natl. Acad. Sci. USA *104*, 8167–8172.

MacKerell, A.D., Bashford, D., Bellott, M., Dunbrack, R.L., Evanseck, J.D., Field, M.J., Fischer, S., Gao, J., Guo, H., Ha, S., et al. (1998). All-atom empirical potential for molecular modeling and dynamics studies of proteins. J. Phys. Chem. B. *102*, 3586–3616.

Mellman, I., and Nelson, W.J. (2008). Coordinated protein sorting, targeting and distribution in polarized cells. Nat. Rev. Mol. Cell Biol. *9*, 833–845.

Mertens, J., Stüber, K., Wunderlich, P., Ladewig, J., Kesavan, J.C., Vandenberghe, R., Vandenbulcke, M., van Damme, P., Walter, J., Brüstle, O., and Koch, P. (2013). APP processing in human pluripotent stem cell-derived neurons is resistant to NSAID-based γ-secretase modulation. Stem Cell Reports *1*, 491–498.

Phillips, J., Braun, R., Wang, W., Gumbart, J., Tajkhorshid, E., Villa, E., Chipot, C., Skeel, R., Kale, L., and Schulten, K. (2005). Scalable molecular dynamics with NAMD. J. Comput. Chem. *26*, 1781–1802.

Prabhu, Y., Burgos, P.V., Schindler, C., Farías, G.G., Magadán, J.G., and Bonifacino, J.S. (2012). Adaptor protein 2-mediated endocytosis of the β-secretase BACE1 is dispensable for amyloid precursor protein processing. Mol. Biol. Cell *23*, 2339–2351.

Rajapaksha, T.W., Eimer, W.A., Bozza, T.C., and Vassar, R. (2011). The Alzheimer's β-secretase enzyme BACE1 is required for accurate axon guidance of olfactory sensory neurons and normal glomerulus formation in the olfactory bulb. Mol. Neurodegener. *6*, 88.

Rajendran, L., and Annaert, W. (2012). Membrane trafficking pathways in Alzheimer's disease. Traffic *13*, 759–770.

Rajendran, L., and Simons, K. (2005). Lipid rafts and membrane dynamics. J. Cell Sci. *118*, 1099–1102.

Rajendran, L., Masilamani, M., Solomon, S., Tikkanen, R., Stuermer, C.A., Plattner, H., and Illges, H. (2003). Asymmetric localization of flotillins/reggies in preassembled platforms confers inherent polarity to hematopoietic cells. Proc. Natl. Acad. Sci. USA *100*, 8241–8246.

Rajendran, L., Honsho, M., Zahn, T.R., Keller, P., Geiger, K.D., Verkade, P., and Simons, K. (2006). Alzheimer's disease beta-amyloid peptides are released in association with exosomes. Proc. Natl. Acad. Sci. USA *103*, 11172–11177.

Rajendran, L., Schneider, A., Schlechtingen, G., Weidlich, S., Ries, J., Braxmeier, T., Schwille, P., Schulz, J.B., Schroeder, C., Simons, M., et al. (2008). Efficient inhibition of the Alzheimer's disease beta-secretase by membrane targeting. Science *320*, 520–523.

Sannerud, R., Declerck, I., Peric, A., Raemaekers, T., Menendez, G., Zhou, L., Veerle, B., Coen, K., Munck, S., De Strooper, B., et al. (2011). ADP ribosylation factor 6 (ARF6) controls amyloid precursor protein (APP) processing by mediating the endosomal sorting of BACE1. Proc. Natl. Acad. Sci. USA *108*, E559–E568.

Sauder, J.M., Arthur, J.W., and Dunbrack, R.L., Jr. (2000). Modeling of substrate specificity of the Alzheimer's disease amyloid precursor protein beta-secretase. J. Mol. Biol. *300*, 241–248.

Schneider, A., Rajendran, L., Honsho, M., Gralle, M., Donnert, G., Wouters, F., Hell, S.W., and Simons, M. (2008). Flotillin-dependent clustering of the amyloid precursor protein regulates its endocytosis and amyloidogenic processing in neurons. J. Neurosci. *28*, 2874–2882.

Selwyn, M.J. (1965). A simple test for inactivation of an enzyme during assay. Biochim. Biophys. Acta *105*, 193–195.

Simons, K., and Ikonen, E. (1997). Functional rafts in cell membranes. Nature *387*, 569–572.

Sinha, S., Anderson, J.P., Barbour, R., Basi, G.S., Caccavello, R., Davis, D., Doan, M., Dovey, H.F., Frigon, N., Hong, J., et al. (1999). Purification and cloning of amyloid precursor protein beta-secretase from human brain. Nature *402*, 537–540.

Stahlschmidt, W., Robertson, M.J., Robinson, P.J., McCluskey, A., and Haucke, V. (2014). Clathrin terminal domain-ligand interactions regulate sorting of mannose 6-phosphate receptors mediated by AP-1 and GGA adaptors. J. Biol. Chem. *289*, 4906–4918.

Sugimoto, I., Futakawa, S., Oka, R., Ogawa, K., Marth, J.D., Miyoshi, E., Taniguchi, N., Hashimoto, Y., and Kitazume, S. (2007). Beta-galactoside alpha2,6-sialyltransferase I cleavage by BACE1 enhances the sialylation of soluble glycoproteins. A novel regulatory mechanism for alpha2,6-sialylation. J. Biol. Chem. *282*, 34896–34903.

Tanzi, R.E. (2005). The synaptic Abeta hypothesis of Alzheimer disease. Nat. Neurosci. *8*, 977–979.

Thinakaran, G., Teplow, D.B., Siman, R., Greenberg, B., and Sisodia, S.S. (1996). Metabolism of the "Swedish" amyloid precursor protein variant in

neuro2a (N2a) cells. Evidence that cleavage at the "beta-secretase" site occurs in the golgi apparatus. J. Biol. Chem. *271*, 9390–9397.

Udayar, V., Buggia-Prévot, V., Guerreiro, R.L., Siegel, G., Rambabu, N., Soohoo, A.L., Ponnusamy, M., Siegenthaler, B., Bali, J., Simons, M., et al.; AESG (2013). A paired RNAi and RabGAP overexpression screen identifies Rab11 as a regulator of β-amyloid production. Cell Rep. *5*, 1536–1551.

Vassar, R., and Kandalepas, P.C. (2011). The β-secretase enzyme BACE1 as a therapeutic target for Alzheimer's disease. Alzheimers Res. Ther. *3*, 20.

Vassar, R., Bennett, B.D., Babu-Khan, S., Kahn, S., Mendiaz, E.A., Denis, P., Teplow, D.B., Ross, S., Amarante, P., Loeloff, R., et al. (1999). Beta-secretase cleavage of Alzheimer's amyloid precursor protein by the transmembrane aspartic protease BACE. Science *286*, 735–741.

Vassar, R., Kuhn, P.H., Haass, C., Kennedy, M.E., Rajendran, L., Wong, P.C., and Lichtenthaler, S.F. (2014). Function, therapeutic potential and cell biology of BACE proteases: current status and future prospects. J. Neurochem. *130*, 4–28.

von Arnim, C.A., Kinoshita, A., Peltan, I.D., Tangredi, M.M., Herl, L., Lee, B.M., Spoelgen, R., Hshieh, T.T., Ranganathan, S., Battey, F.D., et al. (2005). The low density lipoprotein receptor-related protein (LRP) is a novel beta-secretase (BACE1) substrate. J. Biol. Chem. *280*, 17777–17785.

von Kleist, L., Stahlschmidt, W., Bulut, H., Gromova, K., Puchkov, D., Robertson, M.J., MacGregor, K.A., Tomilin, N., Pechstein, A., Chau, N., et al. (2011). Role of the clathrin terminal domain in regulating coated pit dynamics revealed by small molecule inhibition. Cell *146*, 471–484.

Walter, J., Fluhrer, R., Hartung, B., Willem, M., Kaether, C., Capell, A., Lammich, S., Multhaup, G., and Haass, C. (2001a). Phosphorylation regulates intracellular trafficking of beta-secretase. J. Biol. Chem. *276*, 14634–14641.

Walter, J., Kaether, C., Steiner, H., and Haass, C. (2001b). The cell biology of Alzheimer's disease: uncovering the secrets of secretases. Curr. Opin. Neurobiol. *11*, 585–590.

Willem, M., Garratt, A.N., Novak, B., Citron, M., Kaufmann, S., Rittger, A., DeStrooper, B., Saftig, P., Birchmeier, C., and Haass, C. (2006). Control of peripheral nerve myelination by the beta-secretase BACE1. Science *314*, 664–666.

Wong, H.K., Sakurai, T., Oyama, F., Kaneko, K., Wada, K., Miyazaki, H., Kurosawa, M., De Strooper, B., Saftig, P., and Nukina, N. (2005). beta Subunits of voltage-gated sodium channels are novel substrates of beta-site amyloid precursor protein-cleaving enzyme (BACE1) and gamma-secretase. J. Biol. Chem. *280*, 23009–23017.

Yan, R., Bienkowski, M.J., Shuck, M.E., Miao, H., Tory, M.C., Pauley, A.M., Brashier, J.R., Stratman, N.C., Mathews, W.R., Buhl, A.E., et al. (1999). Membrane-anchored aspartyl protease with Alzheimer's disease beta-secretase activity. Nature *402*, 533–537.

Yan, R., Han, P., Miao, H., Greengard, P., and Xu, H. (2001). The transmembrane domain of the Alzheimer's beta-secretase (BACE1) determines its late Golgi localization and access to beta -amyloid precursor protein (APP) substrate. J. Biol. Chem. *276*, 36788–36796.

Zhou, L., Brouwers, N., Benilova, I., Vandersteen, A., Mercken, M., Van Laere, K., Van Damme, P., Demedts, D., Van Leuven, F., Sleegers, K., et al. (2011). Amyloid precursor protein mutation E682K at the alternative β-secretase cleavage β′-site increases Aβ generation. EMBO Mol. Med. *3*, 291–302.

Zhou, L., Barão, S., Laga, M., Bockstael, K., Borgers, M., Gijsen, H., Annaert, W., Moechars, D., Mercken, M., Gevaert, K., and De Strooper, B. (2012). The neural cell adhesion molecules L1 and CHL1 are cleaved by BACE1 protease in vivo. J. Biol. Chem. *287*, 25927–25940.

Cell Reports, Volume *14*

Supplemental Information

Specific Inhibition of β-Secretase Processing of the Alzheimer Disease Amyloid Precursor Protein

Saoussen Ben Halima, Sabyashachi Mishra, K. Muruga Poopathi Raja, Michael Willem, Antonio Baici, Kai Simons, Oliver Brüstle, Philipp Koch, Christian Haass, Amedeo Caflisch, and Lawrence Rajendran

Supplementary information including the methods is available at www.cell.com/cellreports

Supplementary figure Legends

Supplementary Figure 1.

Molecular dynamic simulations of BACE1 and the substrates-analog. (A) Expression of BACE1 substrates at different ages in control (wild type) and transgenic mouse model of AD (Arc/SwAPP mutant). RT-PCR of cortex RNA extracted from healthy or AD mice, 1 male and 1 female mouse in each group. ΔCt = Ct gene – Ct housekeeping. Normalized to 18S and GAPDH, ΔΔCt = ΔCt experimental time point - ΔCt control. X axis: age and y axis: ΔΔCt. (B) Structure and sequence of the octapeptide substrates of wtAPP, swAPP, NRG1, and PSGL1. (C) The active site of BACE1 with the octapeptide of PSGL1 substrate-analog. The snapshot for each BACE1-substrate complex shown is the representative structure of the most populated conformer which was obtained by clustering all MD snapshots by root mean square deviation and a cutoff of 0.8 Å. All C_α atoms of BACE1 except for the loops A, C, D, and F, were used in the structural fitting prior to the clustering. The flap is shown as ribbon while the side chains of BACE1 and substrate as sticks. The carbon atoms of substrate are shown in magenta for clarity. (D) Root mean square fluctuation of $C\alpha$ atoms of BACE1, averaged over intervals of 2 ns after excluding the first 20 ns of each MD trajectory. Black, red, green, blue, and orange represent swAPP, wtAPP, NRG1, PSGL1, and apo complex of BACE1, respectively. Vertical dashed lines indicate the root mean square fluctuation of the catalytic aspartates and the flap residues. The similar RMSF values indicate that the overall plasticity of BACE1 is essentially identical when it is bound to any

of the four substrates. The small fluctuations in the flap region (residue 67 to 77) reflect the stable flap in the presence of substrates in the active site. On the other hand, in the apo form, BACE1 shows a comparatively larger fluctuation in the flap region. Similarly, the catalytic active site (near the regions of the two catalytic Asps - Asp32 and Asp228) also shows small fluctuations representing stable enzyme-substrate complexes. (E) The correlation of fluctuations of the eight substrate C α atoms (shown by different colors in each panel) with the BACE1 C α atoms. The correlation coefficient is obtained from the normalized covariance matrices of the corresponding C α atom displacements which were then averaged over intervals of 2 ns after excluding the first 20 ns of each MD trajectory. The flap region and the two catalytic Asp residues (Asp32 and Asp228) are indicated by vertical dashed lines. The correlated motion of BACE1 and substrate for four complexes show similar correlation pattern where a moderately strong correlation is seen between substrate and the active site, in particular, in the region of two catalytic Asp's (Asp32 and Asp228) and in the flap region which suggests that the four substrates considered here follow a similar binding pattern, and therefore validate further comparison between their binding affinity towards BACE1.

Supplementary Figure 2.

The interaction energy between BACE1 and NRG1, swAPP, PSGL1 and wtAPP derived inhibitors. (A) Time series of the total interaction energy (van der Waals plus electrostatic) between BACE1 and the four inhibitors, i.e., OM99-2 derivative of swAPP, wtAPP, NRG1 and PSGL1, in black, red, green, and blue respectively. Note, (P1') for all four inhibitors is Ala. The order of stabilizing interaction between BACE1 and the inhibitors (NRG1 > swAPP > wtAPP > PSGL1) is similar to that between BACE1 and the corresponding substrates (Figure 1A). (B) Time series of interaction energy between BACE1 and each of

the eight residues of the substrate-analog inhibitors. The residue type is given by one-letter code with the same color as the time series. The Glu residues at P2 and P2' of NRG1 have more favorable interactions than the residues in the other three inhibitors.

Supplementary Figure 3

Chemical structure and ESI-Mass spectra of BACE1 peptide inhibitors. (A) Chemical structures of BACE1 peptide inhibitors having non-coded gamma amino acid statine moieties. (B) ESI-Mass spectra of BACE1 peptide inhibitors a) wtAPP, b) swAPP, c) NRG1 and d) PSGL1. (C) Molecular Characterization of the substrate-derived statine-based inhibitors through electrospray ionization-mass spectrometry (ESI-MS).

Supplementary Figure 4.

Determination of kinetics parameters of NRG1, wtAPP and swAPP reactions with BACE1. The specificity of the different substrates for human recombinant BACE1 was determined by measuring the Michaelis constant K_m and the limiting rate V. The specificity constant K_{cat}/K_m was calculated from these parameters and the enzyme concentration. Progress curves measured at a fixed substrate concentration and three enzyme concentrations showed considerable loss of enzyme activity and did not pass the Selwyn test at reaction times larger than 15 min. This prevented the use of entire progress curves of substrate hydrolysis for calculating kinetic parameters and the initial rate method was used instead.

Supplementary Figure 5.

The endosomally-targeted sterol-linked BACE1 inhibitor does not inhibit NRG1 cleavage in primary neurons. (A) NRG1 β1 type III or GFP (as control for the transduction) was expressed in primary hippocampal/cortical neurons using Lentivirus-mediated transduction,

and cells were treated with the indicated inhibitors TAPI-1, BACE1 inhibitor C3, the endosomally-targeted sterol-linked BACE1 inhibitor, for 24h. Western blotting of Lysates with the Sc-348 antibody to detect full length NRG1 β1 type III and NRG1-CTFs and Conditioned medium was subjected to ECL assay to measure mouse Aβ40 (B). The values are experimental triplicates.

Supplementary Figure 6.

Characterization of iPSC-derived human neurons. Human induced pluripotent stem cell (iPSC)-derived neuroepithelial stem cells express the neural stem cell-associated transcription factors Sox2 and DACH1 as well as the intermediate filament NESTIN (left panel). Following growth factor withdrawal and differentiation for 4 weeks, these cultures form dense neuronal networks (right panel; phase contrast). Scale bars: 200 μm

Supplementary Figure 7.

Amyloid (APP) and non-amyloid BACE1 substrates (NRG1 and L1) have similar detergent insolubility /subcellular localizations in detergent resistant microdomains (DRMs)/ lipid rafts. Western blot analysis of cells expressing either NRG1 β1 type III, L1 or wtAPP subjected to 1% Triton solubility and subsequent separation on sucrose gradient fractionation. DRMs refer to lipid raft fractions and are flotillin-1 positive.

Supplementary Information on Methods

FRET reporters of amyloid and non-amyloid substrates of BACE1

All the Fret reporters (See below tables) were purchased from Bachem. All the FRET peptides contained (7-Methoxycoumarin-4-yl)acetic acid (Mca) and 2,4-Dinitrophenyl (DNP) to serve as fluorophore and a quencher, respectively.

Substrate	Sequence	Catalog number
wtAPP	(Mca-(Asn670,Leu671)- Amyloid Protein Precursor (APP) 770(667-676)-Lys(Dnp)-Arg-Ar-NH_2 trifluoroacetate salt)	M-2460
wtAPP K(P2)E	(Mca-(Asn670,Leu671)- Amyloid Protein Precursor (APP) 770(**K670E**)-Lys(Dnp)-Arg-Ar-NH_2 trifluoroacetate salt)	custom product
swAPP	(Mca-(Asn670,Leu671)- Amyloid Protein Precursor (APP) 770(667-676)-Lys(Dnp)-Arg-Arg-NH_2 trifluoroacetate salt)	M-2465
NRG1	Mca- Ser-Gly- Ile- glu- Phe-Met-Glu-Ala-Glu-Lys(Dnp)-Arg-Arg-NH_2 amide trifluoroacetate salt.	custom product
NRG1 E(P2)K	Mca-Gly- Ile-**Lys**-Phe-Met-Glu-Ala-Glu-Lys(DNP)-Arg-Arg-NH2 trifluoroacetate salt	custom product
PSGL1	Mca-Ser-Ala-SerAsn-Leu-Ser-Val-Asn-Tyr(Dnp)-arg-Arg-NH_2 trifluoroacetate salt.	custom product

Substrate	Sequence	Calatog number
L1	Mca-Ser-ASP-THR-ASP-TYR-GLU-ILE-HIS-LEU-Lys(Dnp)-Arg-Arg-NH2 trifluoroacetate salt	custom product
L1 E1087K	Mca-Ser-ASP-THR-ASP-TYR-LYS-ILE-HIS-LEU-Lys(Dnp)-Arg-Arg-NH2 trifluoroacetate salt	custom product

Synthesis of substrate-analog inhibitors derived from BACE1 substrates

Inhibitors	Sequence	Catalog number
wtAPP	Glu- Val- Lys- Met- φ[CHOH-CH2] - Asp- Ala- Glu- Phe	see method
swAPP	Glu-Val-Asn-Leu- φ[CHOH-CH2] -Asp-Ala- Glu- Phe	see method
NRG1	Gly- Ile-Glu-Phe- φ[CHOH-CH2] -Met-Glu-Ala-Glu	see method
PSGL1	Ala-Ser-Asn-Leu- φ[CHOH-CH2] -Ser-Val-Asn-Tyr	see method

Transition-state mimic 8-residue peptide inhibitors (see above table) were designed based on the BACE1-binding region in the substrates. The scissile peptide bond is replaced with an isostere moiety to render the peptide bond non-cleavable. The BACE1 substrate-derived peptide inhibitors (Supplementary Fig. S3a) were synthesized by conventional manual solid-

phase peptide synthesis, employing standard Fmoc chemistry protocols (Chan and White, 2000). In brief, syntheses were done at 100 μ M scale, the respective preloaded 2-chlorotrityl resins (0.5-0.8 mmol/g) were swollen in DCM/DMF and couplings were carried out using HBTU/DIEA/DMF. Five-fold excess of Fmoc-amino acids were used for each coupling. The deprotection of Fmoc group was achieved by 20% piperidine in DMF. The washings were done by DMF after each step in the coupling cycle and in the final cycle DCM and methanol washings were performed. The synthesised peptides were cleaved from dried resins by TFA-TIS-Water cocktail mixture (95:2.5:2.5) and precipitated in precooled TBME. The N- and C-termini free peptides were collected after centrifuges and TBME wash cycles. The crude peptides were subjected to HPLC purification by reverse phase C18 column, using acetonitrile-water (containing 0.1% TFA) as gradient solvent system. The fractions were collected, lyophilized and the molecular integrity is confirmed by ESI-MS analysis (Supplementary Fig. S3b). Supplementary Fig. S3C summarizes the molecular characterization by ESI-MS. The observed molecular masses [M+H]+ and [M+Na]+ are very well matches with calculated mass of these peptides, confirming their chemical integrity. All preloaded resins, Fmoc-amino acids, reagents and solvents were purchased from Merck-NovaBiochem, Germany and Fmoc-Statine was purchased from PolyPeptide Laboratories, France.

Fmoc - 9-Fluorenylmethoxycarbonyl

Stat - (3S,4S)-4-amino-3-hydroxy-6-methyl-heptanoic acid

DCM - Dichloromethane

DMF - Dimethylformamide

HBTU - O-(Benzotriazol-1-yl)-N,N,N′,N′-tetramethyluronium hexafluorophosphate

DIEA - Diisopropyl ethyl amine

TFA - Trifluro acidic acid

TIS - Triisopropyl silane

TBME - tert-Butyl methyl ether

ESI-MS- Electrospray ionization Mass spectrometry

HPLC - High Performance Liquid Chromatography

Real-Time PCR

RNA was isolated from mouse cortical brain tissue at the ages of 1 day, 1 month, 3 months, 6 months, 9 months and 12 months from wild type (WT) and Tg (Arc/SwAPP) mice. Tissue samples were homogenized by titration in 1 ml Trizol using 18G, 22G and 26G gauge needles to sequentially dissociate the tissue. RNA was extracted following the Trizol protocol, according to manufacturer's guidelines. RNAs were further purified using Qiagen RNeasy kit including on column DNAseI digestion. RNA was eluted into the RNA storage solution (AM7001; Ambion). RNA quality and concentration were determined by Agilent Bioanalyser and Nanodrop Spectrophotometer. Real-time PCR (RT-PCR) was carried out by reverse transcribing 5ug of total RNA using first strand cDNA synthesis Kit (11904-018; Invitrogen) according to manufacturer's instructions. Briefly, the cDNA was then diluted 1:5 in a TaqMan-Low density array (Applied Biosystems) and PCR was performed according to manufacturing protocol.

Cell Lines and Cultures

Human embryonic kidney cells (HEK293T), HEK 293 stably expressing BACE1 (kind gift from Prof. D. Selkoe), HeLa Kyoto, HeLa-GalT-GFP were cultured in low-glucose DMEM (Invitrogen) containing 10% FBS, penicillin (100 U/ml) and streptomycin (100 μg/mL) in a humidified 5% CO2 atmosphere.

Confocal Microscopy

Images were acquired on a Leica TCS/SP8 confocal microscope (Leica, Wetzlar, Germany) with a 63Å~ water immersion objective. A 543 nm HeNe laser was used to excite Cy3 (HYD window: 553– 600 nm). A 633 nm HeNe laser was used to excite Cy5 (HYD window: 655– 710nm).

Transferrin and EGF receptor endocytosis

Transferrin uptake experiments were performed as described in Kamioke et al,. 2004 (1). Briefly, HeLa Kyoto cells or HEK cells were transfected with Dyn WT or Dyn K44A plasmids. 24h post transfection, cells were serum-starved in DMEM for 1 h, non transfected cells were treated with 35uM Pitstop2 (Abcam, ab120687) during the serum starvation step, and incubated with 25 μg/ml Alexa 546-conjugated transferrin or 100nM of Alexa 633-conjugated EGF receptor for 20 min at either 37 °C or 4 °C (control). After rinsing three times with PBS and reducing surface labeling using 50 mM deferoxamine mesylate-containing buffer (150 mM NaCl, 2 mM $CaCl_2$, and 25 mM sodium acetate/acetic acid, pH 4.5), cells were fixed with 4% paraformaldehyde (PFA), in PBS and subjected to fluorescence imaging.

Shiga toxin and endosomally-targeted sterol-linked BACE1 inhibitor uptake

HeLa-GalT-GFP and HeLa cells were plated tow days prior to treatment (4000 cells). The day of experiment cells were washed twice with serum free medium then incubated with 2ug/ml of Alexa 633-conjugated Shiga toxin or 2uM of rhodoamine -conjugated endosomally sterol-linked BACE1 inhibitor on ice for 45 min (2). Then cells were washed 3 times with full serum medium and incubated at 37°C for 0, 5, 20 30 and 1 hour. Cells were then washed tree time with PBS and fixed with 4% PFA, in PBS. For the colocalization of the sterol-linked BACE1 inhibitor with EEA1 and Lamp1, after PFA fixation, cells were

permeabilized with 0.02% Triton for 5 min and blocked with 2% BSA for 1 hour at room temperature. Anti-EEA1 (Abcam1/400) and anti-Lamp-1 (Santa cruz 1/100) were applied over night at 4°C. After washing, secondary antibody 633-conjugated anti-mouse antibody 1/400 was applied for 1hour at room temperature, cells were then washed and DNA stained with DAPI for 10 min. After mounting cells were subjected to fluorescence imaging.

For immunocytochemical characterization of iPSC-derived neuronal cultures, cells were washed with PBS and fixed with 4% paraformaldehyde (PFA, 10 min, RT), blocked in 0.1% Triton X-100 (Sigma) and 10% FCS in PBS, incubated with the primary antibodies (16 hours, 4°C), washed with PBS, counterstained with secondary antibodies (1 hour, RT) and DAPI and mounted with Mowiol.

Mutagenesis, cell transfection and inhibitor treatments

NRG1 β1 type III, and wtAPP mutants were obtained using the quick-change site-direct mutagenesis kit according to the manufacturer's protocol (Stratagene 200519). HEK 293 stably expressing BACE1 cells were transfected using 1μg of DNA and 2 μl of Lipofectamine 2000 (Invitrogen) -according to the manufacturer's instructions for 24-well plate -with pcDNA or the needed plasmid. 24 hours post-transfection, cells were treated with DMSO, 5 μM of C3 (beta-secretase Inhibitor IV, 565788; Calbiochem) 20 μM TAPI-1 (579051; Calbiochem), 20 μM GL189 (565780; Calbiochem) or 500 nM endosomally-targeted sterol-linked BACE1 inhibitor for 12 hours. Endosomally-targeted sterol-linked BACE1 inhibitor was replenished every 4 hours. Lysates were used for western blotting and cells supernatants were used for ECL assays whenever is needed.

Cell viability

Cell viability was assessed using Alamar Blue assay (10 % v/v Alamar Blue) according to the manufacturer's instructions (BUF012B; AbD Serotec). Absorbance was monitored at the end of the reaction (after 4 h) and spectroscopically read at wavelengths of 544nm and 590 nm (Spectra Max Gemini XS, Molecular devices).

***In vitro* BACE1 solubilized membrane assay**

Four 10 cm dishes of HEK 293 stably expressing BACE1 cells were transfected with NRG1β1 Type III and were washed with PBS, scraped in 1 ml PBS and centrifuged for min at 8000 rpm. Cell pellets were resuspended in 700 µl buffer H (20 mM HEPES, 150 mM NaCl, 10% glycerol, 5 mM EDTA, pH 7.4) and the solution drawn 20 times through a 3 ml syringe with 20 gauge needle. Unbroken cells were removed by centrifugation at 4000 rpm for 5 min. In order to obtain P2 fractions, the supernatant was centrifuged at 55000 rpm for 1 h and 4°C. Membrane fractions were washed once in 300 µl incubation buffer (0.1 M Na Acetate pH 4.0, 10 µg/ml Leupeptin, 1 µg/ml Aprotinin, 1 mM PNT and 5 mM EDTA) and resuspended in 100 µl incubation buffer in absence or presence of 5 µM C3 or 500 ηM sterol linked BACE1 inhibitor. After incubation for 4 h at either 0°C or 37°C, the samples were loaded on 4-12% BisTris SDS-PAGE gel and investigated by Western blot analysis.

Isolation of detergent-resistant microdomains(DRMs)/ lipid rafts

1 T75 flask of 80-90% confluent cells was lysed for 30 minutes in cold in TNE (10mM Tris HCl, pH 7.5, 150mM NaCl, and 5 mM EDTA) buffer with 1% Triton X-100, protease and phosphatase inhibitors. The solution after lysis was further homogenized with ten strokes in a loose fitting dounce homogenizer and centrifuged at 900 g for 10 minutes. 1ml of the cleared supernatant was mixed with 1ml of 85% sucrose in TNE buffer and layered at the bottom of a Beckman 12 ml centrifuge tube. The lysate was overlaid with 6 ml of 35% sucrose in TNE buffer and finally with 3.5ml of 5% sucrose in TNE buffer. The samples

were centrifuged in a SW41 rotor at 200,000 g for 20 h at 4°C. At the end of the run, 1ml fractions were collected from the top of the gradient. 50 µl from each of the fractions was boiled with SDS buffer and subjected to a reducing 4–12% gradient SDS PAGE and western blotting analysis.

Sample preparation and Western blotting

To obtain total cell lysate, cells were washed with ice-cold PBS twice, lysed for 30 min on ice in lysis buffer: 2% NP-40, 0.2% SDS in PBS, supplemented with protease inhibitors (Roche) and post-nuclear supernatant was obtained by centrifugation (20 min, 1200 x g, 4°C**).** Protein concentration was determined with BCA protein assay (Pierce) and equal amount of protein (30-50 µg) was subjected to SDS-PAGE analysis. Proteins were transferred onto nitrocellulose membrane (Protran; Whatman) and the indicated antibodies were used for immunodetection. Bound antibodies were detected with HRP-conjugated secondary antibodies using the chemiluminescence detection reagents ECL (GE Healthcare).

Antibodies

The following antibodies were used for immunoblotting: antibody to NRG1 C-terminus (pRb, 1:1000 Sc-348; Santa Cruz biotechnology), to NRG1-β-CTF (rat, 1:40, monoclonal neoepitope-specific antibodies, 4F10; from Dr. Michael Willem), to L1, anti C-terminal antibody (rabbit, 1:50000, PcytL1; from Prof. Peter-Hans Altevogt). HRP-conjugated secondary antibodies (rat, mouse and rabbit, 1:15000; GE Healthcare). Primary antibodies and concentrations for immunocytochemical characterization of iPSC-derived neuronal cultures were as follows: Sox2 (1:500, R&D Systems), Nestin (1:600, R&D Systems), Dach1 (1:100, Proteintech), beta-III tubulin (1:2000, Covance), Map2ab (1:250, Chemicon),

GFAP (1:1000, DakoCytomation). Secondary antibodies were Alexa488 anti-ms, Alexa555 anti-ms, Alexa488 anti-rb and Alexa555 anti-rb (all 1:1000, Life Technologies).

Supplementary References:

(1) Kamioke et al., (2004). A Novel Dynamin-associating Molecule, Formin-binding Protein 17, Induces Tubular Membrane Invaginations and Participates in Endocytosis, J Biological Chemistry. Vol. 279, No. 38, Issue of September 17, pp. 40091–40099,
(2) Rajendran, L. et al. (2008). Efficient Inhibition of the Alzheimer's Disease β-Secretase by Membrane Targeting, Science 320, 520-523.

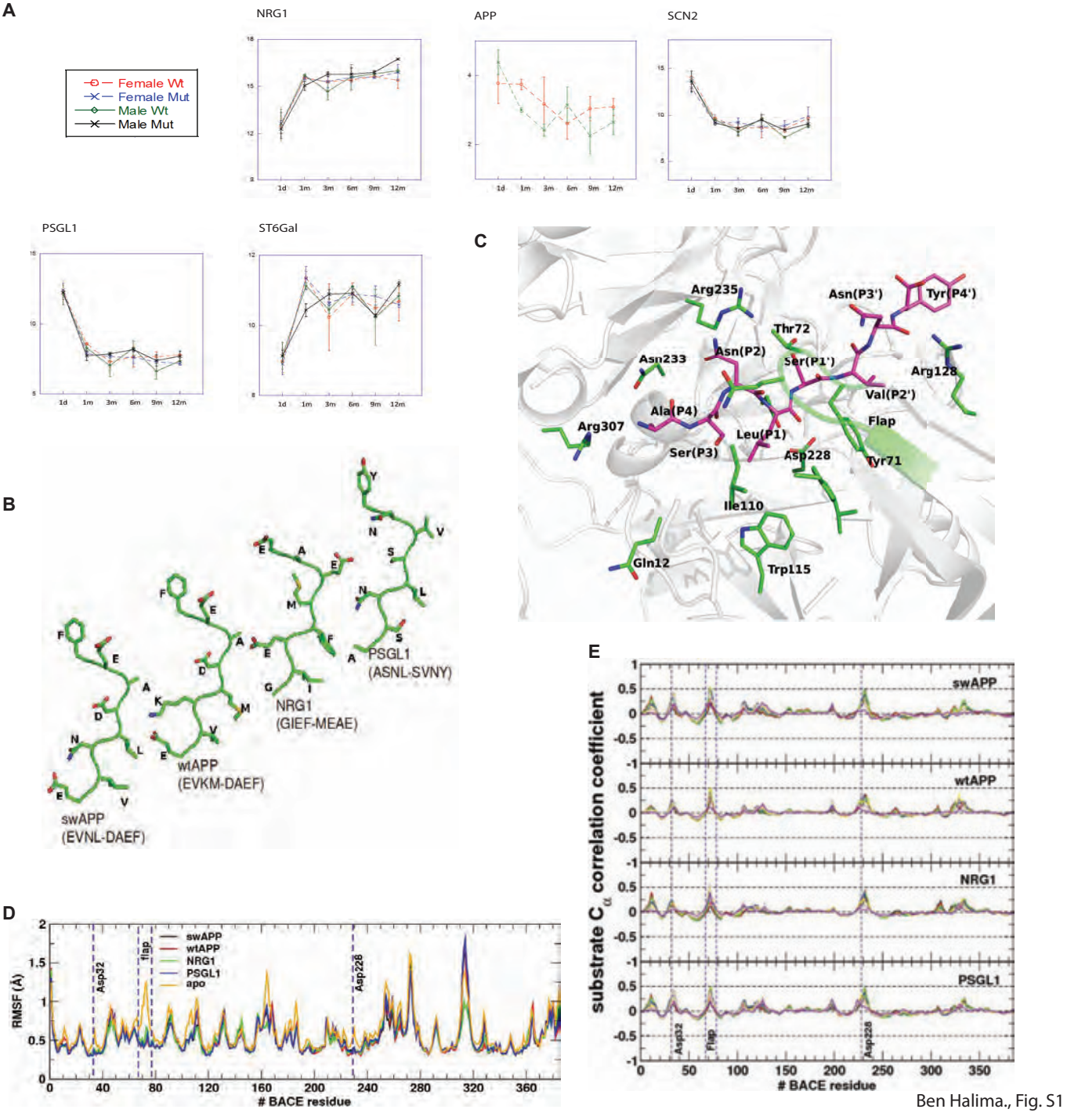

Ben Halima., Fig. S1

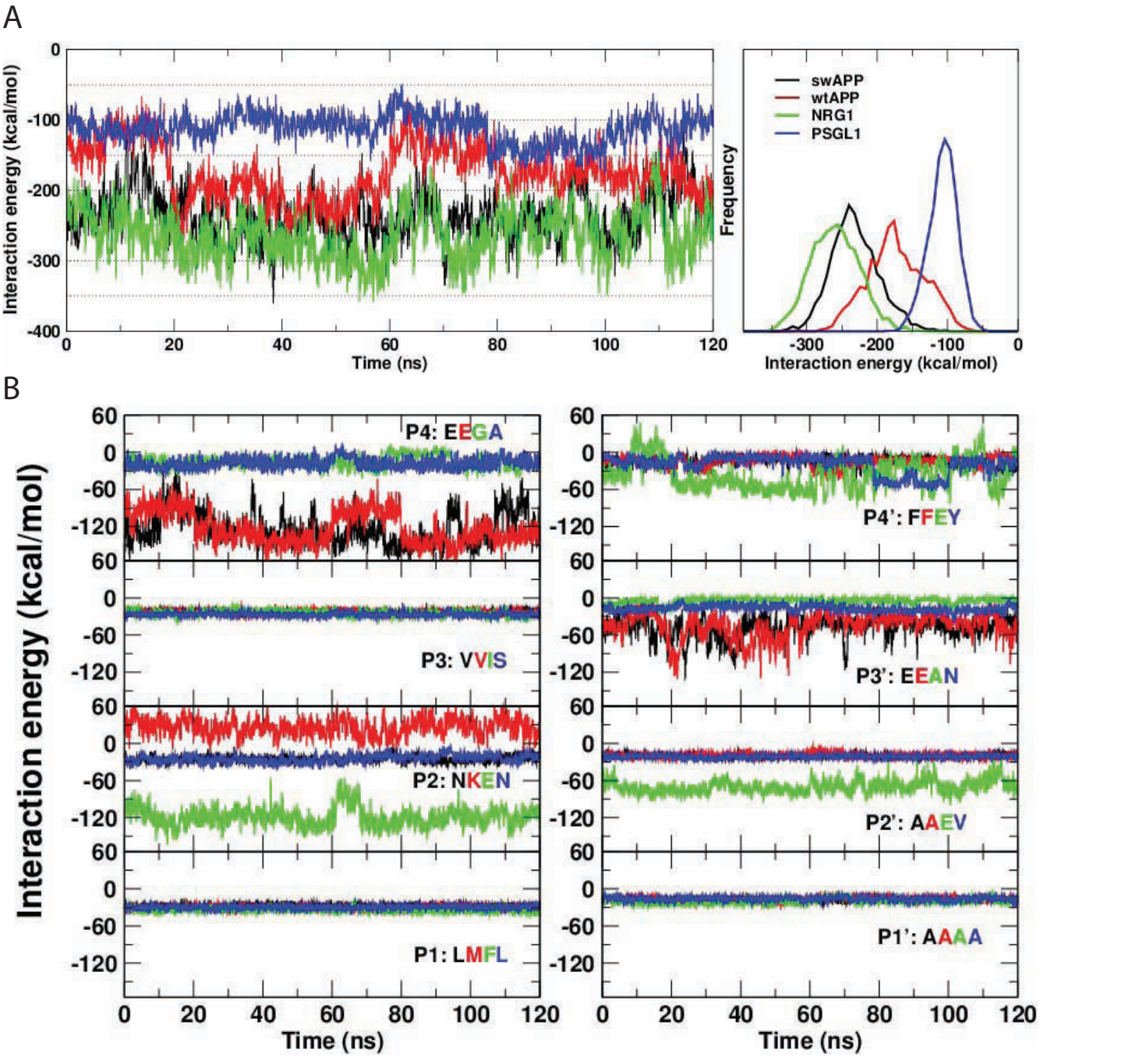

Ben Halima., Fig. S2

A

wtAPP

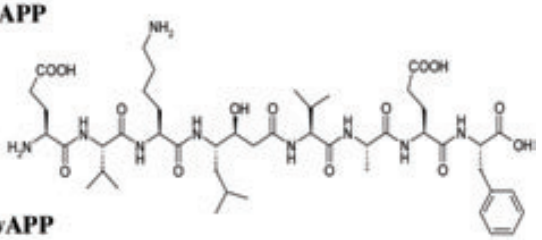

swAPP

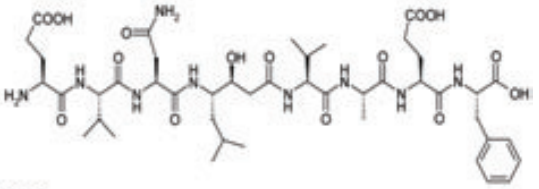

NRG1

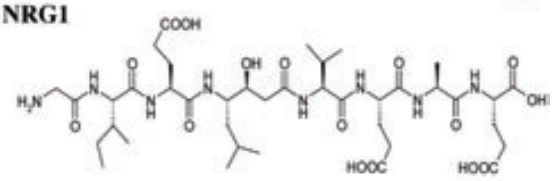

PSGL

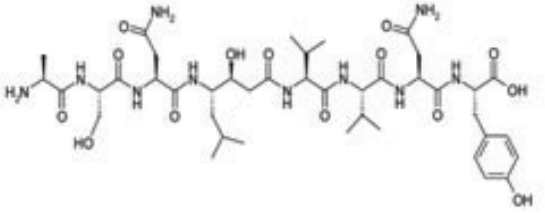

B

wtAPP

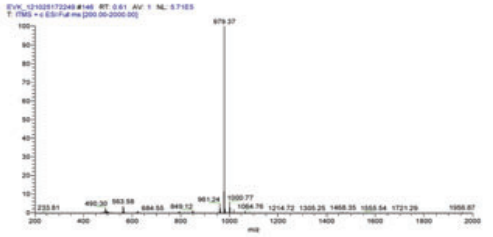

swAPP

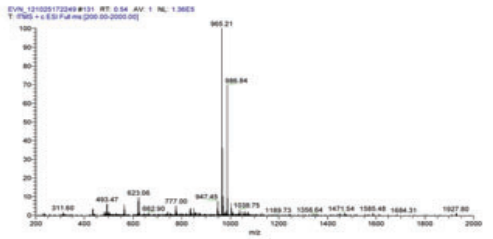

NRG1

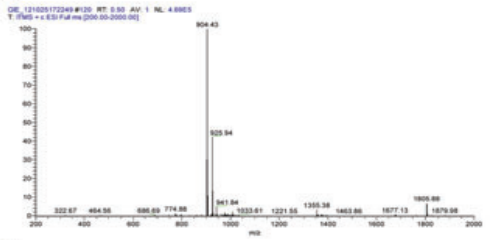

PSGL

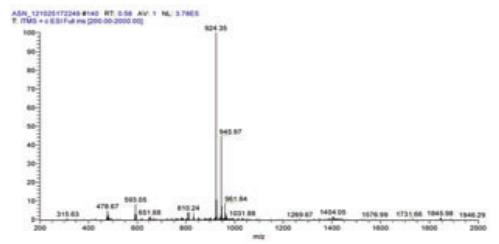

C

Substrate peptide	Calculated $[M]_{avg}$ (Da)	Observed $[M+H]^+$ (Da)	Observed $[M+Na]^+$ (Da)	Observed $[M+2H]^{+2}$ (Da)
wtAPP	978.15	979.37	-	-
swAPP	964.08	965.21	986.84	-
NRG1	902.99	904.43	925.94	-
PSGL	923.03	924.35	945.97	-

Ben Halima et al., Fig. S3

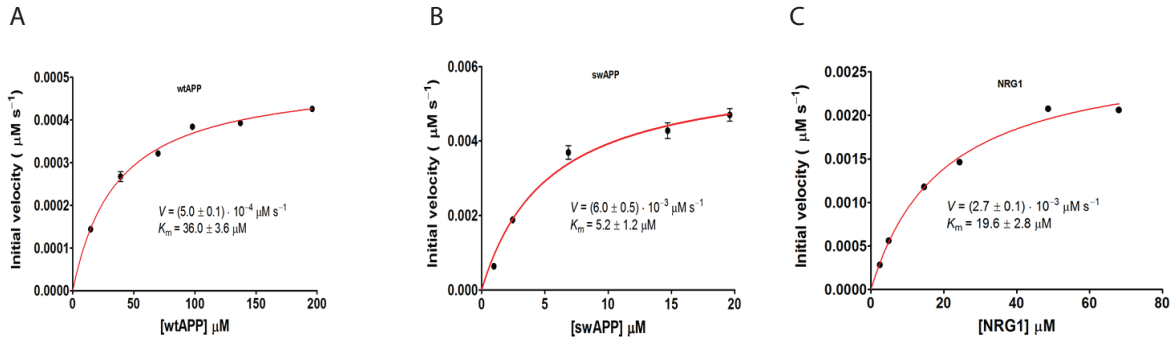

Ben Halima., Fig. S4

A

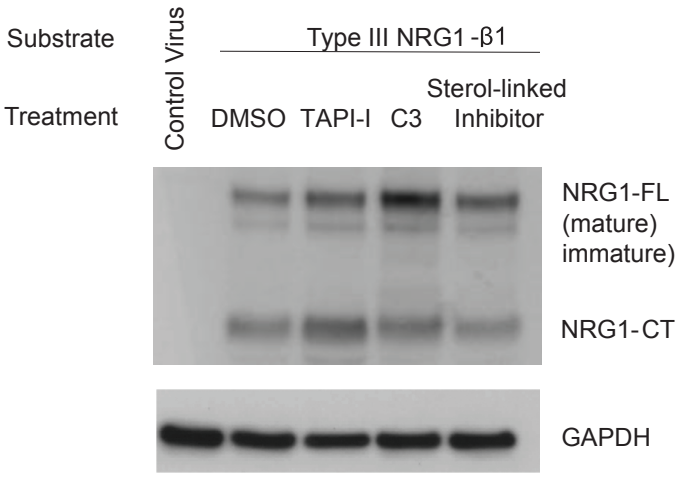

B

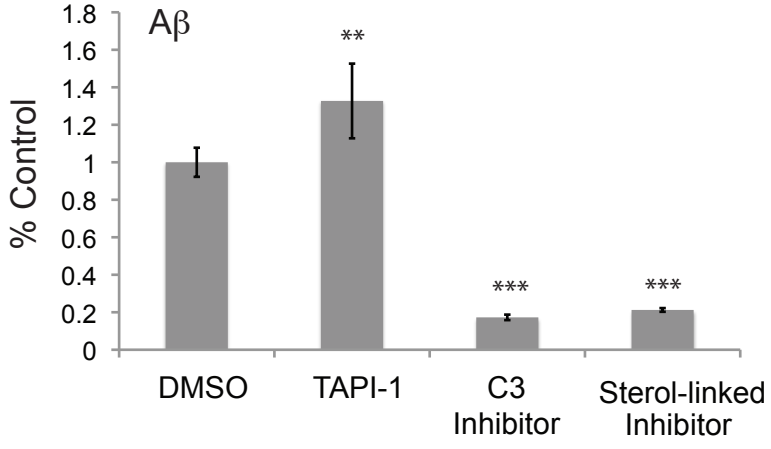

Ben Halima., Fig. S5

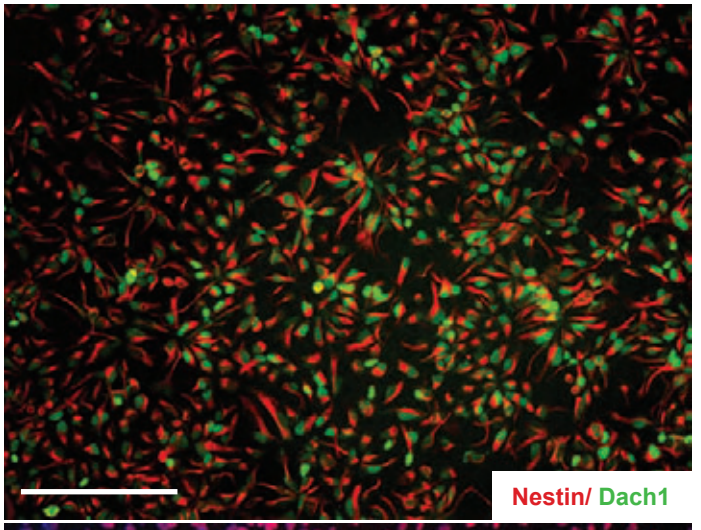

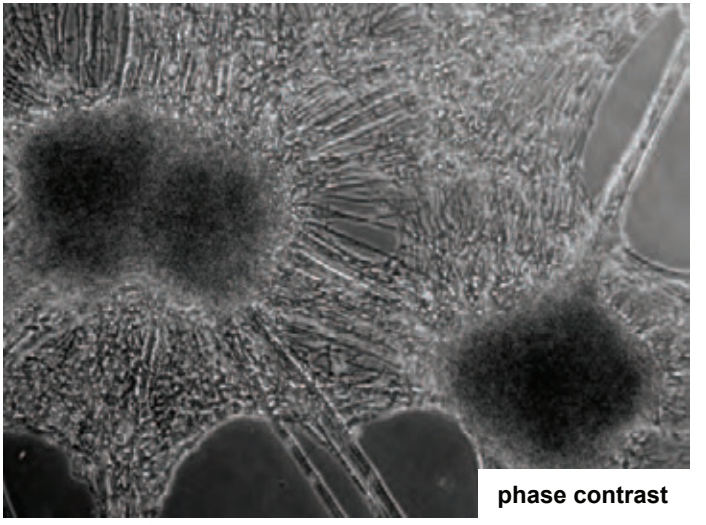

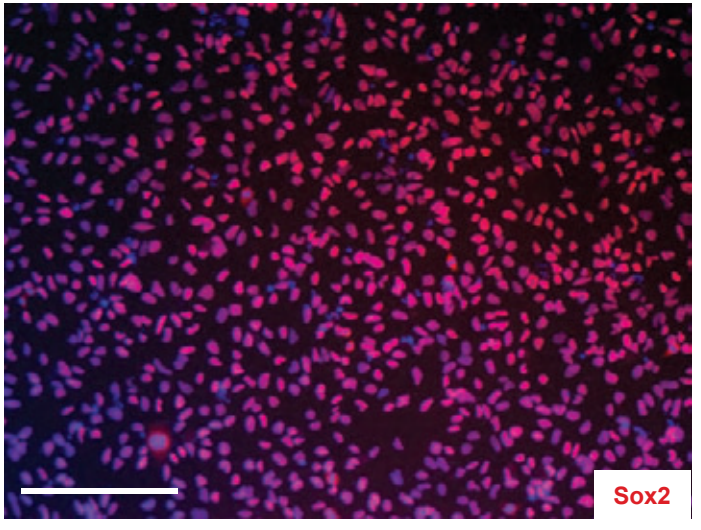

Ben Halima., Fig. S6

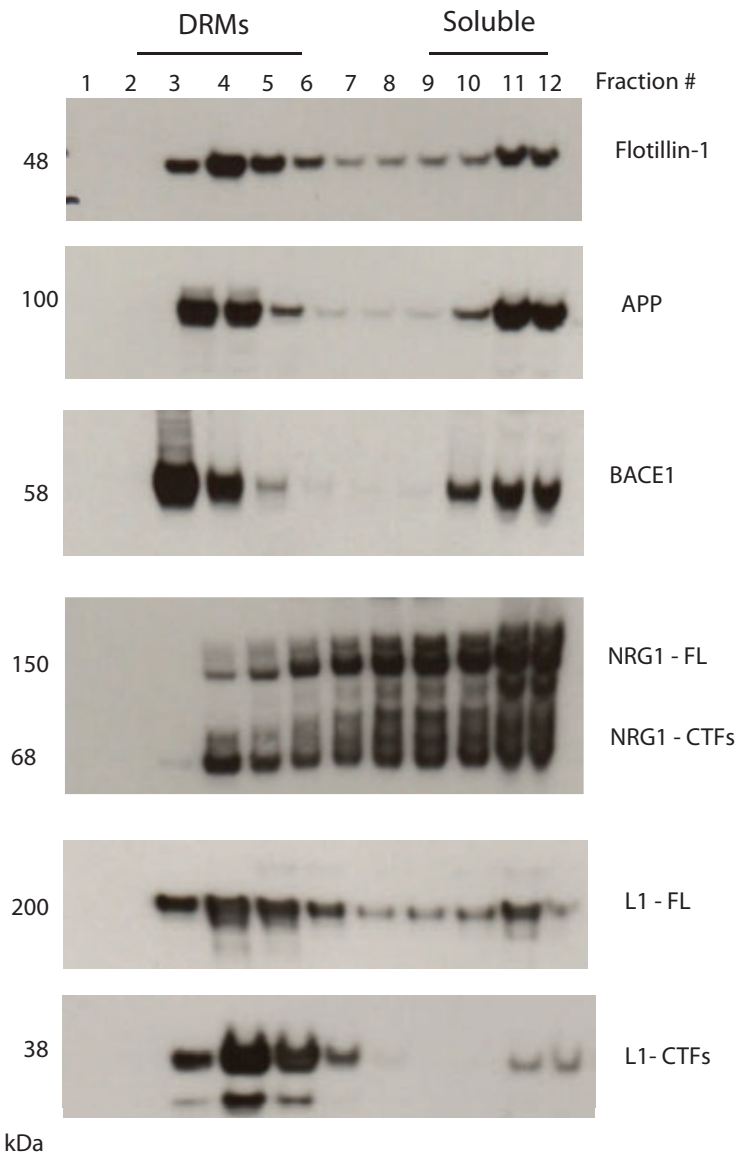

Ben Halima et al., Fig. S7

Inventory of Supplemental information

1. **Supplementary Figure 1**
Molecular dynamic simulations of BACE1 and the substrates-analog (Related to Main figure 1)

Figure S1 shows the details and provide the controls of the MD simulations between BACE1 and the substrates-analog conducted in **Figure1**.

2. Supplementary Figure 2: The interaction energy between BACE1 and NRG1, swAPP, PSGL1 and wtAPP derived inhibitors. (Related to main figure 1)

Figure S2 shows the details and provide the controls of the MD simulations between BACE1 and the substrates derived inhibitors conducted simulations are conducted in **Figure 1)**

3. Supplementary Figure 3: Chemical structure and ESI-Mass spectra of BACE1 peptide inhibitors. (Related to main figures 2 and 3)

Figure S3 provides information about the substrates-derived inhibitors used in **Figure 2 and 3**. Also provides further mass spectrometry information about the substrates derived inhibitors used in **Figure 1**.

4. Supplementary Figure 4: Determination of kinetics parameters of NRG1, wtAPP and swAPP reactions with BACE1. (Related to main figures 2 and 4)

Figure S4 gives the kinetics parameters that were used for the calculations for **Figure 2C**.

5. Supplementary Figure 5: The endosomally-targeted sterol-linked BACE1 inhibitor does not inhibit NRG1 cleavage in primary neurons. (Related to Figure 4)
Figure S5 shows the validation of the endosomally-targeted sterol-linked BACE1 inhibitor in a different cellular type than in **Figure 4**. **(Related to main figures 4 and 5)**

6. Supplementary Figure 6: Characterization of h-iPSCs. (Related to main igure 6)

Figure S6 provides the characterization of the h-iPSCs used in the assay of **Figure 6**.

7. Supplementary Figure 8: Amyloid (APP) and non-amyloid BACE1 substrates (NRG1 and L1) have similar detergent insolubility /subcellular localizations in detergent resistant microdomains (DRMs)/ lipid rafts. (Related to Figure 7)

Figure S7 shows the subcellular localization of BACE1, APP, NRG1 and L1 to lipid rafts as suggested by the reviewer. **(Related to main figure 7)**